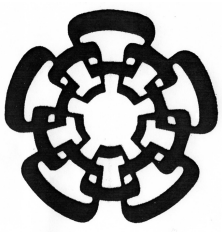

CENTRO DE INVESTIGACIÓN Y DE ESTUDIOS
AVANZADOS DEL INSTITUTO POLITÉCNICO NACIONAL

UNIDAD ZACATENCO

PROGRAMA DE MAESTRÍA EN CIENCIAS EN
SISTEMAS AUTÓNOMOS DE NAVEGACIÓN AEREA Y SUBMARINA

"Drone Coaxial dentro de una Proteccion Gimbal: Diseño, Modelado, Control y Resultados Experimentales"

T E S I S

Que presenta:

ERIC AMIDZAEL BAZÁN HERNÁNDEZ

Para obtener el grado de:

MAESTRO EN CIENCIAS
EN SISTEMAS AUTÓNOMOS DE NAVEGACIÓN AEREA Y SUBMARINA

Directores de la Tesis:

Dr. Rogelio Lozano Leal
Dr. Gerardo Ramón Flores Colunga

México, D.F. Abril, 2015

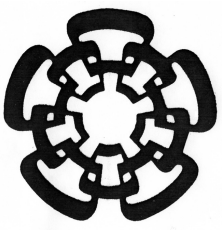

CENTRO DE INVESTIGACIÓN Y DE ESTUDIOS
AVANZADOS DEL INSTITUTO POLITÉCNICO NACIONAL

CAMPUS ZACATENCO

MASTER SCIENCE PROGRAM IN
AERIAL AND SUBMARINE AUTONOMOUS NAVIGATION SYSTEMS

"Coaxial Drone inside a Gimbal protection: Design, Modelling, Control and Experimental Results"

T H E S I S

Presented and defended by

ERIC AMIDZAEL BAZÁN HERNÁNDEZ

To obtain the degree of

MASTER IN SCIENCE

IN AERIAL AND SUBMARINE AUTONOMOUS NAVIGATION SYSTEMS

Thesis directors

PhD. Rogelio Lozano Leal
PhD. Gerardo Ramón Flores Colunga

Mexico City April, 2015

Acknowledgements

It is a pleasure to express my gratitude to all the people who have helped me the last two years of master degree and have been an important part of my life.

First of all, I am forever thankful to my parents Leonardo Bazán and Ana Bertha Hernández, my sister Ana Jocelyn Bazán and my girlfriend Gabriela Quezada for all of your love and specially for all your support.

I thank my advisor and friend in Compiègne France and also in Mexico City, Gerardo Flores, for supporting me all the way in my master's thesis; I have learned many things from him. I am incredibly grateful for the time and dedication he has had all this time.

I am equally thankful to the SANAS program coordinator, PhD. Sergio Salazar, and to my advisor, PhD. Rogelio Lozano, for the encouragement and support to do the studies and the mastery stay in Compiègne, France.

I also thank my friends, Hector Escamilla for all adventures in Europe and in Mexico and Jonathan Flores for their advices and for sharing so many experiences together.

I am particularly grateful to Jorge Torres from CINVESTAV, who has honored me by agreeing to be a member of the jury of this thesis.

A warm thanks goes to all collegues from whom I have learned a lot from the good coffee breaks and discussions we had: Héctor Escamilla (UTC-CINVESTAV), Hilario Salazar (UTC-BUAP), Mariano Larios (UTC-BUAP), Diego Mercado (CINVESTAV-UTC), Isrrael Lugo (UTC), Shuting Zhou (UTC). Specially I am thankful to Logan who helped me out when I was leaving France.

Finally, I am thankful to the National Council of Science and Technology (CONACYT) for gave to me the financial support to accomplish this thesis.

Eric Bazán

Mexico City, April 2015

Contents

List of Figures

List of Tables

Resumen

Esta tesis presenta una configuración novedosa de un Vehículo Micro Aéreo (MAV por sus siglas en inglés): el robot aéreo *LaBola*. Este vehículo tiene la peculiaridad de estar compuesto por dos estructuras principales; la primera, un helicóptero en configuración coaxial que se encuentra dentro de una segunda estructura, una protección Gimbal que permite que el helicóptero sea resistente a la presencia de impactos mientras que al mismo tiempo el drone mantiene la maniobrabilidad con la que cuentan los multirotores estándar. El diseño, construcción, el estudio de los sensores abordo y la programación del vehículo son desarrollados inicialmente en la Universidad Tecnológica de Compiègne y después en el Centro de Investigación y de Estudios Avanzados del Instituto Politécnico Nacional. Además, un control de seguimiento de orientación acotado para *LaBola* que es desarrollado en el Grupo Especial ortogonal $\mathsf{SO}(3)$ se investiga, teniendo en cuenta el hecho de que los actuadores tienen límites físicos de saturación. Se muestra que la estrategia de control propuesta garantiza la estabilidad exponencial, y que tiene la capacidad de seguir las maniobras de giro con grandes ángulos de orientación. El rendimiento de la estrategia de control se prueba en simulaciones numéricas y experimentos en tiempo real, validando con éxito la eficacia de los enfoques propuestos.

Palabras clave

Helicoptero coaxial. Sistema gimbal. Modelado. Estabilidad. Contol basado en Lyapunov. Sistema no lineal. Grupo especial ortogonal. $\mathsf{SO}(3)$.

Abstract

This thesis introduces a novel Micro Aerial Vehicle (MAV) configuration: *LaBola* air robot. This vehicle has the peculiarity of being composed of two main structures; the first, a helicopter in coaxial configuration which is inside a second structure, a Gimbal protection which allows the helicopter overcomes the presence of impacts while at the same time maintaining the manoeuvrability which feature standard multirotors. The design, construction, study of onboard sensors and vehicle programming are initially developed at the Technological University of Compiègne (UTC) and then an the Centro de Investigación y de Estudios Avanzados del Instituto Politécnico Nacional (CINVESTAV). Furthermore, a bounded attitude tracking control for *LaBola*, developed in the Special Orthogonal Group $\mathsf{SO}(3)$ is investigated, considering the fact that the actuators have physical saturation limits. It is shown that the proposed control strategy guarantees exponential stability, and has the capability of tracking rotational maneuvers with large attitude angles. The performance of the control strategy is tested in numerical simulations and real-time experiments, successfully validating the effectiveness of the proposed approaches.

Keywords

Coaxial helicopter. Gimbal system. Modelling. Stability. Lyapunov-based control. Non-linear system. Special orthogonal group. $\mathsf{SO}(3)$.

1

Introduction

Contents

1.1 Motivation and Challenges

In the last decade flying robots have been evolved from being the dreams of science fiction to mature aerial sensor platforms deployed in an increasing variety of applications [1], [2]. Recent advances in the miniaturization of electronics and sensors driven by the mobile computing industry, along with the constant evolution of energy storage and composite materials, have enabled even smaller hovering platforms. Despite of infamous for their use by the military, Micro Aerial Vehicles (MAVs) are increasingly being used in civilian applications as diverse as aerial photography and photogrammetry [3], automatic detection of forest fires [4] and even the transportation of medical samples in rural Africa [5] or just for deliver things bought on a e-shop as Amazon [6]. In all of these applications flying robots navigate in open, obstacle free environments and have access to precise localization data through Global Positioning Systems (GPS). Flight as locomotion is particularly interesting in the exploration of damaged buildings as it can provide human operators with an elevated viewpoint of places otherwise inaccessible to people. Flying robots are not constrained by the morphology of the ground and can be used to navigate across rubble, through staircases or up elevator shafts much quicker than ground-based robots.

Based on the foregoing, practical applications for the aerial exploration of cluttered environments are common. For example, on March 11, 2011 a tsunami destroyed large portions of the Japanese coast and rendered a nuclear power plant unstable.

High levels of radiation kept human rescuers from entering the plants, and ground robots had trouble surmounting the large amounts of rubble on the ground. A single Honeywell T-Hawk UAV was used for aerial imagery outside the plant, but was unable to penetrate inside the plant due to its large size. In February of the same year an earthquake in Christchurch, New Zealand, caused extensive damage to the city. This scenario was one of the first uses of a flying robot inside a building in a disaster situation, rescuers used a commercially-available Parrot AR.Drone [7] to fly into a collapsed church to assess the damage inside, that were unable to venture beyond the large open church hall. MAVs have also been proposed for use in mine rescue and recovery [8], but nevertheless there are also current limitations: in theory, MAVs could be used for the Side Entry scenario, while in practice it is still uncertain how they could operate in total darkness and avoid protrusions from the roof, indeed, as opposed to flight outdoors and in large open spaces, indoor flight posses several additional challenges to navigation. Precise positioning is difficult due to the absence of GPS along with low visibility due to smoke or lack of light. The presence of a large number of irregular obstacles and the fragility of current flying systems to any impact, make the survival in such an environment for most flying systems a very hard task .

To defeat the challenge of flying among of the obstacles many works [9–12] has been developed using vision or distance sensor or advanced techniques using localization and mapping (SLAM) to avoid obstacles. Unfortunately, in these scenarios where there are always situations in which the clutter is too dense, the visual conditions are too poor due to the lighting and color, or the obstacles are quite complex to be

detected due to its texture. Collisions are unavoidable just using vision techniques or sensor information. Even robust robots which can fly in aggressive/acrobatic mode, or those having a large number of sensors for navigation, are not able to avoid all collisions because in these environments are often bright objects like windows, low-contrast scenarios, or unexpected situations, such as moving obstacles (animals) or sensor failure.

It is proposed to make a vehicle with special attention in the mechanical design in order to endure collisions in case of lack of sensor information. Some solutions are given to this problem. Platforms equipped with frames that protect sensitive elements like sensors and propellers from impacts have recently developed but its protective structures are useful only indoors [13] when one axis is affected by a collision, and it depends on the control strategy selected. However, some impacts can affect the roll, pitch and yaw axes of flying platforms, which may cause a fall to the ground because the propulsion system generates accelerations toward undesired directions and may not be able to generate lift.

1.2 State of Art

1.2.1 Protective Frames

As opposed to withstand collisions, most approaches taken so far in indoor flying robotics have looked at actively avoiding them. Several sensor modalities have been proposed for detecting obstacles of varying sizes. In the simplest cases, one or several discrete distance sensors pointed in specific directions can be used to detect the global presence of an obstacle. Infra-red (IR) triangulation [14] or ultrasonic (US) [15] sensors have been used for obstacle avoidance, but are relatively heavy and have high power requirements, and are thus ill-suited for flying platforms in large numbers.

Based on the foregoing, some aerial vehicles have paid special attention in the design of special mechanisms for protecting the MAV frame in order to endure collisions caused by for example, lack of sensor information. Some existing solutions to collision protection can be categorized in two types of structures: stiff bump protection and flexible protection. Stiff protection is the most common strategy and is sufficient for protecting spinning propellers from low-energy contact. Commercial platforms, such as Quanser Qball-X4 [13] (Figure 1.1e) or Ascending Technologies Firefly [16] (Figure 1.1a), come with *indoor flight kits*, which essentially are rigid protections mounted on the frame to protect sensitive elements like sensors and

propellers from impacts; this protective structures are useful only when one axis is affected by a collision. Some MAVs have a three dimension protection having the capability to protect from impacts in all directions. Among this kind of aerial robots is the single-rotor helicopter presented in [17] that is surrounded by a cage made of carbon tubes (Figure 1.1b); the spherical robot built at the Japan Ministry of Defence (JMD)[18] (Figure 1.1d) or the Vision'Air [19] (designed specifically for big collisions); or the platform Gimball [20] inspired by the collision resistance of insects. There are others protections with original design as the platform called MAVion [21], the HyTAQ robot [22] from the Illinois Institute of Technology (IIT) (Figure 1.1c), or the Parrot Mini drone Rolling Spider [23] that features two wheels protecting the rotors from impacts and also can be used to roll on the ground, along the wall or even ceiling while it is flying. On the other hand, soft protection typically takes the form of either compressible materials such as foam or deformable cages made up of thin components such as carbon fibre rods. A typical example is the mobile-phone-controlled AR.Drone [7] (Figure 1.1f) which has a 2 cm-thick foam hull to protect its propellers. A styrofoam frame is also used by the Distributed Flight Array [24] (Figure 1.1g), a unique flying robot made of individual single-propeller modules that cannot fly by themselves but can connect to other modules and thus create different multi-rotor systems. Foam is an improvement to stiff protection, as it increases absorption distance and distributes the force over a larger area. Its low stiffness, however, make it inefficient for absorbing large amounts of energy. The protection around the AR.Drone, for example, increases the 370 g platform's weight by 60 g, but a force of only 6 N results in a deformation of the structure, sufficient to contact the propeller [25]. A further disadvantage to

foam is its fragility, though it may survive several collisions, but repeated impacts progressively reduce the energy it can absorb. Another popular protective structure solution is using one or several flexible carbon rods to absorb collision energy. Compared to foam, carbon is stiffer for a similar weight and is thus more efficient in absorbing energy. The quadrotor presented in [14] (Figure 1.1h) uses a single rod for propeller protection which it is only dimensioned for minor bumps and would not survive a high-speed collision. The commercial multi-rotor FanCopter (Figure 1.1j) extends this idea to several rods around the platform for better protection. Finally, the Hopping Rotochute [26] (Figure 1.1i), a hybrid flying-jumping platform, completely surrounds its two coaxial rotors with a carbon fibre cage, protecting it from contact in all directions. The use of bent circular springs around a platform has the advantage of absorbing collision energy through several interconnected springs instead of a single one but a major disadvantage of such a system, however, is that the rods used to produce the cage are sourced as straight rods and must be bent into a circular shape, storing energy that cannot be recovered until the cage is disassembled. As every material has a maximum strain it can absorb, this initial strain reduces the additional collision energy that the rods can absorb before failure and is thus not an efficient use of the material. A second problem arises from their manner of deflection; when a circular spring contacts a flat surface it creates inflection points which have higher radius of curvature than the rest of the spring, and thus induce failure caused by stress.

(a) Ascending Firefly.

(b) Single-rotor helicopter.

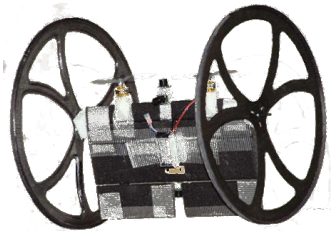

(c) Mavion.

(d) Spherical drone by the JMD.

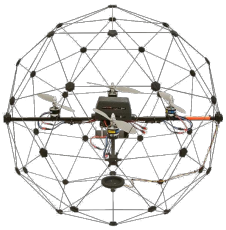

(e) Quanser Qball.

(f) AR. Drone.

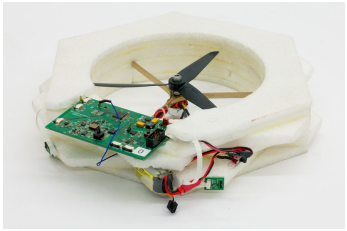

(g) Distributed flight array.

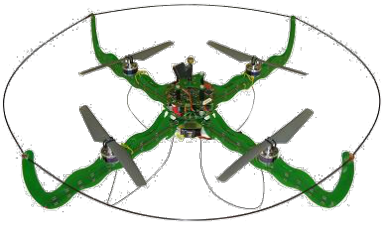

(h) Quadrotor using carbon fibre rods.

(i) Hopping Rotochute.

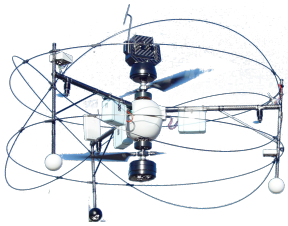

(j) Fancopter.

Figure 1.1: Some examples of the different types of protection mechanisms used on flying robots. From 1.1a-1.1e, robots that use a rigid frame and stiff protection mechanisms to survive low-intensity contact. From 1.1f-1.1j, robots that use flexible protection mechanisms to absorb collision energy.

1.2.2 Mechanical Configuration of the MAV

Many researchers have changed their motivation from developing large outdoor UAVs to discovering the potential of miniature indoor MAVs. Nowadays there is a particular interest in the vehicles rotary wing as they are multirotors (quadrotors, hexarotors, etc) because the study of this type of air vehicles is widely developed, however, several configuration types exist, like a single main rotor and a tail rotor configuration, tandem rotor configuration, a side-by-side configuration rotors rotors and a coaxial configuration [27] which are little studied due to their mechanical complexity.

Among the MAVs, one could find some complex machines as the helicopters. Their complexity is due to the versatility and maneuverability to carry out all type of tasks (i.e. vertical, translational and hover flight, etc.), this is the case of work done in [28] where is proposed a helicopter in classic configuration as well as a non-linear three degrees of freedom mathematical model to represent such helicopter in vertical flight (take-off, climbing, hover, descent and landing).

Other works preferred remove the tail rotor which has the classical helicopter configuration and control the torque generated by the main rotor and the lateral displacement of the vehicle through control surfaces governed by servomotors, obtaining a hybrid configuration [29]. Such studies propose a very similar modelling to that of classic helicopters with the difference that the forces causing the displacement of the helicopter are generating by control surfaces while the thrust

force is obtained as a single-rotor vehicle by the moment theory briefly entered in Section 2.3.

There are other works that propose a coaxial helicopter configuration within which you can identify two main configurations: Coaxial helicopters that control the lateral movement of the vehicle by a swash-plate [30], [31], [32], [33], [34] [35],[36] (like the classic helicopter) and those who control the lateral displacement by control vanes [18], [37], [38], [39]. In both cases, the torque produced by the propulsion system is cancelled because each rotor rotates in opposite directions. Within the same branch (coaxial helicopter), there are some platforms that seek to innovate the displacement mechanism. For example, the CoaX platform [40], which manages the movement of the vehicle by manipulating the center of gravity through a mass attached to the frame of the body or the UH platform that has three rotors; the first two are in contra rotative coaxial configuration and are exclusive to generate the lift force, while the third rotor, is partially responsible for generating the thrust force and completely responsible of the vehicle displacement through a swash plate [41].

All previous works and others mentioned in [42] mostly have a modelling of forces and moments generated in the body, while others only have practical results, this due to how recent was the subject at that that time, however, nowadays inhomogeneity presented in mathematical models, especially corresponding to the thrust force provided by coaxial motors, has generated a poor modelling that does not consider all the proper factors to be taken under a coaxial configuration. This issue will be addressed in chapter (chapter thurst) in order to propose a

modelling that includes most aerodynamic characteristics presented in the coaxial configuration.

1.2.3 Rotational Representations and Attitude Control Approaches

In the recent past, the design and implementation of control algorithms for autonomous helicopters has been the object of a relevant research, due to an identified need for manoeuvrable autonomous aerial vehicles, for both military and civilian applications. Also, the attitude dynamics of a rigid body appears in various engineering applications, such as aerial and underwater vehicles, robotics, and spacecraft. Despite the substantial interest in MAV's (see section 1.1), little attention has been paid to constructing nonlinear control systems for them, particularly to designing nonlinear tracking controllers.

In recent works, feedback linearization techniques have been applied to helicopter models. The main difficulty in the application of such techniques is the fact that, the helicopter dynamics are not directly input-output linelizable. However, it is possible to find good approximations to the helicopter dynamics such that the approximate system is input-output linearisable [43]. The feedback linearisation apporoach suffers from the fact that, since the attitude is parametrized using Euler angles [44], singularities arise when performing some maneuvers, such as loops, barrels rolls, split-s, etc, i.e., when representing complex rotational maneuvers of a MAV, thereby fundamentally restricting their ability to track nontrivial trajectories.

A possible solution to the singularity problem is represented by chart switching when approaching a singularity but these generates high gains in the proximity of singularities.

Another way to solve the singularity problem is using the quaternion representation. Quaternions do not have singularities, but they have ambiguities in representing an attitude, as the three-sphere and the unit-vectors is in R^4. Therefore, a single physical attitude of a rigid body may yields two different control inputs, which causes inconsistency in the resulting control system. It is possible to construct continuous controllers, but they may exhibit unwinding behavior, where the controller unnecessarily rotates a rigid body through large angles, even if the initial attitude is close to the desired attitude, thereby breaking Lyapunov stability [45]. An attitude control system based on quaternions is applied to a quadrotor UAV in [46].

Geometric control, as utilized in this work, is concerned with the development of control systems for dynamic systems evolving on nonlinear manifolds that cannot be globally identified with Euclidean spaces [47], [48]. By characterizing geometric properties of non-linear manifolds intrinsically, geometric control techniques provide unique insights to control theory that cannot be obtained from dynamic models represented using local coordinates [45]. This approach has been applied to fully actuated rigid body dynamics on Lie groups to achieve almost global asymptotic stability [49], [50], [51].

One of the distinct features of the configuration manifold of attitudes is that it evolves on a non-linear manifold, referred as the special orthogonal group SO(3).

This yields important and unique properties that cannot be observed from dynamic systems evolving on a linear space.

1.3 Thesis Objective

Design and built a innovative flight robot enable for flight in cluttered, difficult indoor/outdoor environments, i.e, create a vehicle capable not only to remain stable in vertical flight, but also to be able to provide collisions resistance in a smooth way, is the goal of this thesis. To achieve this objective, we proposed a MAV with a protective frame taking advantage of the characteristics of a gimbal system. This proposition brings about the main focus of the thesis: If contact with obstacles is unavoidable, then the platform must be designed to survive and recover from this contact. There are three main challenges resulting from this conclusion:

- **Robustness to Contact:** The mechanical structure of the platform must be robust to repeated physical contact with the environment, whether from the slightest brush against a wall to a high-energy impact resulting from a free-fall from an elevated position. Such mechanism protection will be designed, build and test in order to ensure the collision resistance.

- **Self-Recovery:** Surviving a collision is only useful if the platform can keep flying. It must be able to return to the air from any possible landing position.

This point could be reached implementing a control law capable of avoid the singularities and ambiguities, making possible to take off again from any position after a crash.

- **Integration with Flight Systems:** The most challenge task is to integrate robustness and self-recovery into a platform that is still capable of flying. This requires minimizing the weight and power requirements of the additional mechanisms and placing them intelligently within the structure of the platform to limit their effect on the platform's centre of gravity (COG) and aerodynamics. Furthermore, it requires a extensive study of avionics, in hardware and software, to relate the mechanical structure whit the electronics onboard.

Only after the flying platform can consistently absorb multiple bumps with walls and objects and take off again after falling will it be able to fulfil complex missions in real human environments truly autonomously. The size of the platform is limited to <100 cm in its largest dimension in order to navigate within an environment originally intended for use by humans and as such features hallways, doorways, windows and stairwells. Due to the motor features and the fact that higher weight translates higher-energy impact, there is a limit the weight of the platform and thus this thesis focuses on a low-weight platform.

1.4 Thesis Outline

This thesis brings together elements from such varied fields of knowledge as mechanical engineering, aerodynamics, electronics, robotics and control theory to design a small flying platform capable of navigating cluttered environments currently inaccessible to robots. This thesis is organized around the design, modelling and control of such platform, and the subsequent contributions that are presented.

After a first chapter of introduction, Chapter 2 presents the mathematical model for a coaxial helicopter with special emphasis on the thrust's model, that is, making emphasis on the aerodynamic facts involved in a MAV of the described characteristics. An exhaustive research was made due to the lack of the uniqueness in the literature on this topic. Immediately, a proposed control law developed in the special orthogonal space which takes into account the saturation limits of the actuators is denoted in Chapter 3. Some experimental results and simulations whose validate the stiffness of the mechanism protection and also that shows the convergence of the bounded control law re shown in Chapter 4. After that, Chapter 5 is dedicated to describe the configuration, components and subsystems responsible of making fly and stabilizing the designed *LaBola* including the characteristics of the gimbal protection and the materials used in the built of both frames; the coaxial MAV and its protection. In Chapter 6 concludes the thesis and reiterates the main conclusions that were drawn in the work. Also, the outlook a perspectives of the project are given in order to exhorting the continuation of this work.

2

Modelling of the Platform *LaBola*

In this Chapter, the mathematical model of the proposed platform is described. Such model is addressed from two different approaches and studies the aerodynamic effects caused by coaxial configuration and how they affects the forces and moments generated in the vehicle, specially in the thrust force given by the brushless motors and the propellers. This modelling is essential for developing the control law. The Chapter is organized as follows. In Section 2.2 the equations of motion of a rigid body and other essential terms are introduced. A detailed aerodynamic thrust model in hover for the proposed platform is covered in Section 2.3 giving a interference factor induced by the separation of the rotors. In Section 2.4 a description of the aerodynamic forces and moments applied on the coaxial helicopter are presented.

Contents

2.1 Introduction

There are several kinds of aircraft structures that have been used in indoor flight by robotic researchers. The most common types are light fixed-wing planes, single-rotor helicopters and multirotors.

Conventional single-rotor helicopters use a main rotor to generate lift and a tail rotor to balance the torque caused by main rotor rotation. Motions of a single-rotor helicopter are mainly controlled by a swash plate that is linked to the main rotor, this swashplate changes the collective pitch and cyclic pitch of the main rotor through servomotors letting the helicopter to move in six degree of freedom; such mechanism causes strong cross-coupling between control inputs and the steering of single-rotor helicopter is difficult due to its coupled dynamics. In addition, exposed tail rotor blades have a high possibility to collide with something in an indoor environment.

Multirotors use N rotors to achieve stable hovering and flight. These rotors can be enclosed uniformly to avoid collision between them and the mass can be distributed from the center of mass to make the helicopter easier to control. The rotors have fixed pitch, i.e., there is no needed to use servomotors to generate motion; the movements are controlled by difference of forces generated by changing the velocity of the rotors.

In these work, a helicopter in coaxial configuration using two rotors rotating in

opposed direction to cancel the torque, is used due to the advantages over the other types of platforms, summarized as follows:

1. It is proven to be more power efficient as compared to the single-rotor or quad-rotor configurations [42].

2. It has higher maximum forward speed than a single-rotor helicopter since it always has a pair of advancing and retreating blades, creating a symmetric lift in forward flight [52].

3. It has higher payload to dimension ratio than all the other configurations[36].

4. Coaxial design has more a compact structure without tail rotor and can provide stronger thrust with two main rotors.

5. Main rotor blade collision can be avoided with a protection frame that surrounds the helicopter.

One disadvantage of the coaxial helicopter is the increased mechanical complexity; the rotor hub needs to be carefully designed to drive two counter rotating rotors, notwithstanding, this problem can solved by purchasing a commercial product instead of creating our own.

2.2 Equations of Motion

As usually in aerodynamics, an inertial frame $\mathcal{I} = (e_{x_\mathcal{I}}, e_{y_\mathcal{I}}, e_{z_\mathcal{I}})$ and a body-fixed frame $\mathcal{B}(e_{x_\mathcal{B}}, e_{y_\mathcal{B}}, e_{z_\mathcal{B}})$ are introduced [53]. The non-linear rigid body dynamics is considered, therefore the equations of rotational and translational dynamics are given by [53], [54]:

$$\begin{aligned} \dot{\xi} &= \upsilon \\ m\dot{\upsilon} &= Rf^b - mge_{z_\mathcal{I}} \\ \dot{R} &= R\hat{\Omega} \\ J\dot{\Omega} &= -\Omega \times J\Omega + \tau^b \end{aligned} \tag{2.1}$$

where $\xi \in \mathbb{R}^3$ represent the position and $\upsilon \in \mathbb{R}^3$ the velocity of the robot, $J \in \mathbb{R}^{3\times3}$ its the inertia matrix, $\Omega \in \mathbb{R}^3$ its angular velocity, $\hat{\Omega}$ the skew symmetric matrix associated with Ω and $f^b \in \mathbb{R}^3$ and $\tau^b \in \mathbb{R}^3$ are the forces and torques applied on the vehicle, respectively, represented with respect of the fixed-body frame. For this work, it is assumed that the mass m is constant and $ge_{z_\mathcal{I}}$ is the gravitational force, where $e_{z_\mathcal{I}} = (0, 0, 1)$ is a unit vector. The configuration of the rigid body is the orientation of the body-fixed frame with respect to the inertial frame, and it is represented by a rotation matrix $R \in SO(3)$, where $SO(3)$ is the group of 3×3 orthogonal matrices with determinant 1, i.e., $SO(3) = \{R \in \mathbb{R}^{3\times3} | R^T R = I, detR = 1\}$. In equation (2.1), there is a *hat* map $\wedge : \mathbb{R}^3 \to \mathfrak{so}(3)$ which is a operator that maps a vector in $\mathbb{R}^3$ onto the corresponding Lie algebra elements, namely, a 3×3 skew-symmetric

matrix. More explicitly

$$\forall x = [x_1, x_2, x_3]^T \in \mathbb{R}^3, \quad \hat{x} = \begin{pmatrix} 0 & -x_3 & x_2 \\ x_3 & 0 & -x_1 \\ -x_2 & x_1 & 0 \end{pmatrix}$$

There exist the inverse of the hat map which is denoted by the *vee* map $\vee : \mathfrak{so}(3) \to \mathbb{R}^3$. These operators have several properties summarized as follows:

$$\hat{x}y = x \times y = -y \times x = -\hat{y}x, \tag{2.2a}$$

$$tr[A\hat{x}] = \frac{1}{2} tr[\hat{x}(A - A^T)] = -\hat{x}(A - A^T)^\vee, \tag{2.2b}$$

$$\hat{x}A + A^T\hat{x} = (\{tr[A]I_{3\times 3} - A\}\hat{x})^\wedge, \tag{2.2c}$$

$$R\hat{x}R^T = (Rx)^\wedge, \tag{2.2d}$$

for any $x, y \in \mathbb{R}^3, A \in \mathbb{R}^{3\times 3}$, and $R \in SO(3)$.

2.3 Thrust Modeling

There are two principal approaches to face the aerodynamic of a helicopter rotor: the Momentum Theory (MT) or disk actuator theory and the Blade Element Theory (BET). The first approach which was proposed by W.J.M. Rankine (1865), Alfred George Greenhill (1888) and R.E. Froude (1889), describes a mathematical model of an ideal actuator disk such as a propeller or helicopter rotor and the

simplest way to apply MT and predict thrust and power of a single rotor,this is, when the helicopter is in hover and applying the fundamental assumption that the rotor can be idealized as an infinitesimally thin actuator disk [55], because the air flow is axisymmetric. This is the easiest flow regime to analyze. On the other hand, the Blade Element Theory (BET) designed by William Froude (1878), David W. Taylor (1893) and Stefan Drzewiecki, is the second approach that attacks the problem from the point of view of propeller behavior. Both approaches are usually combined in order to provide additional relationships necessary to describe the induced velocity on the rotor disk [56], [57].

At the begin, both approaches were used only for single rotor vehicles but due to the increasing use of coaxial rotor systems, it caused the development of MT and BET for coaxial rotor systems, giving a fundamental aerodynamic analysis of a contra-rotating coaxial system. However, the design of a contra-rotating coaxial system implies peculiar issues that a simple rotor does not have, such as the separation distance and load sharing between the rotors, wake structure, solidity effects, performance, influence between rotors, etc. A good summary of different approaches has been made showing theoretical and experimental results of dynamic analysis of coaxial systems in [42].

Two important conclusions mentioned in [42] prompted the investigation for a correct thrust model: The Russian approach, especially the experiments done by A.D. Levin reports that *the averaged aerodynamic characteristics of a coaxial configuration are practically independent of the distance between the rotors.* Also, its experiments concludes that *the distance between rotors in the coaxial*

configuration affects only the distributions of thrust between the upper and lower rotors as consequence, a coaxial rotor in axial flight could be treated as an equivalent solidity single rotor.

On the other hand, studies and experiments done by Nagashima and others [42], propose that coaxial rotor wake could be optimized with an appropriate selection of rotor parameters, such as rotor diameter, solidity of the rotor, blade chord, number of blades and the rotor spacing. By analyzing both actuators discs (upper and lower motor), the resulting model takes account that the inner part of the lower motor experiments a downwash from the upper motor and the outer part experiments an upwash, implying the existence of a relationship between the axial and rotational velocities in the wakes of a hovering coaxial rotor. The principal contribution of this approach is the interference factor obtained from the BET and MT theory applied to a coaxial system, this factor is well known and useful to study the coaxial systems performance as presented in [58–60]. Also, this interference factor could be reached experimentally building a platform as in [36] giving interesting results for a specific rotor and blade configuration.

The study of these approaches were highly important in order to find the closest thrust model for the conter-rotating motor used in the vehicle, since the influence of each blade on themselves could be different and deliver different performance results that vary as in [61].

2.3.1 A Single Rotor Helicopter in Vertical Flight

Starting by the MT of a single rotor helicopter, depicted in Figure 2.1 we can observe the principal zones or planes that a rotor has in hovering flight. Cross section *0* denote the far upstream plane of the rotor, cross sections *1* and *2* are the planes just above and below the rotor disc, respectively, and the cross section ∞ denote the downstream of the rotor at infinity; it is called far wake or *vena contracta* of the rotor.

From [57] we consider the actuator disk area A and the total thrust T (see Fig. 2.1). It is assumed that the loading is distributed uniformly over the disk. Let v_i the induced velocity at the rotor disk and w the wake induced velocity infinitely far downstream, also v_i and w are assumed uniform over the slipstream section. The rotational energy in the wake due to the rotor torque is neglected: the fluid is incompressible and inviscid. The mass flux through the disk given by

$$\dot{m} = \rho A v_i \tag{2.3}$$

is constant along the wake by conservation mass. Thus since the flow far upstream is at rest for the hovering rotor the thrust force is given by

$$T = \dot{m} w \tag{2.4}$$

and the work done per unit time or power consumed by the rotor is given by

$$P = Tv_i = \frac{1}{2}\dot{m}w^2 \tag{2.5}$$

From equations (2.3), (2.5) and (2.4), there exist a relation between the induced velocity at the rotor disk v_i and the wake induced velocity given by w, $v_i = \frac{1}{2}w$. By now, it is possible to relate the rotor thrust at the rotor disk by using (2.4)

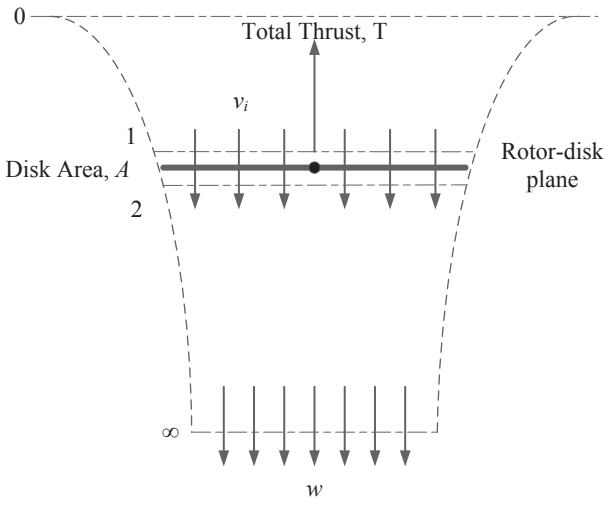

Figure 2.1: Flow model for momentum theory analysis of a simple rotor in hovering flight.

Rearranging this equation and solving for the induced velocity at the plane of the rotor disk it follows that

$$v_i \;=\; \sqrt{\frac{T}{2\rho A}} = \sqrt{\left(\frac{T}{A}\right)\frac{1}{2\rho}} \tag{2.6}$$

From (2.6) we can observe two facts: the ratio $\frac{T}{A}$ known as disk loading, which is

an important parameter in helicopter analysis, and that the velocity needed to maintain the vehicle in hover is the same, i.e., $v_i \equiv v_h$. After that, it is possible express the induced power P_i to maintain a vehicle in hover with a single rotor system. Therefore it follows that

$$P_i = Tv_i = Tv_h = T\sqrt{\frac{T}{2\rho A}} = \frac{T^{\frac{3}{2}}}{\sqrt{2\rho A}} \tag{2.7}$$

2.3.2 A Coaxial Rotor Helicopter in Vertical Flight

For a coaxial counter-rotating system, G. Leishman and S. Ananthan in [62] carried out a complete study working with MT, BET and Flow Vortex Momentum (FVM) expressing the behavior of each of these approaches. They presented four principals configurations or cases in which a coaxial contra-rotative system could be represented. These cases are presented next.

- Case 1: The two rotors rotate in the same plane, o very nearly as in practise, they operate at the same thrust (see Fig. 2.2).

- Case 2: The two rotors rotate in the same plane but are operated at a balanced, equal and opposite torque (see Fig. 2.2).

- Case 3: The rotors are operated at the same thrust but the lower rotor operates in the fully slipstream, i.e vena contracta, of the upper rotor (see Fig. 2.3).

- Case 4: The rotors are operated at balance torque with the lower rotor operating in the vena contracta of the upper rotor (see Fig. 2.3).

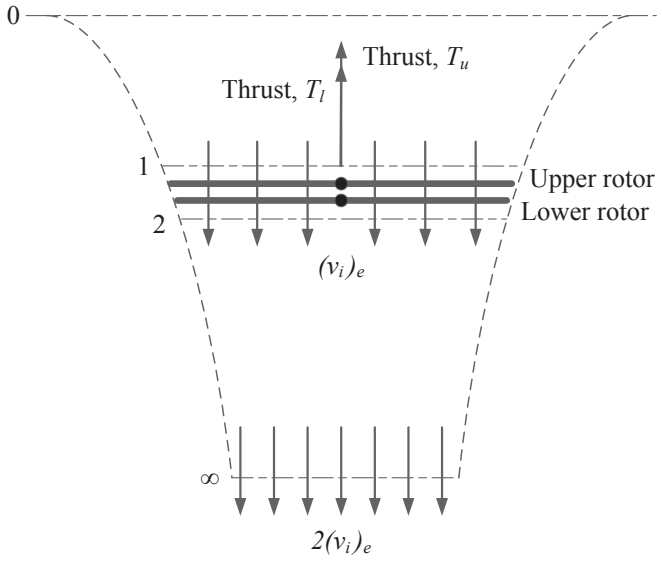

Figure 2.2: Flow model of a coaxial rotor system with both rotors rotating in the same plane.

In practice, the space between blades is part of the design of a coaxial rotor vehicle; they are spaced enough far apart to prevent inter-rotor blade collisions so, the lower motor always works in the vena contracta of the upper rotor [62]. In this work, the attitude control of the vehicle is not achieved by changing the pitch and roll angles of the lower blade, so the distance between them is fixed, that allows to choose between case 1 and 2. The case 2 fits well to describe the trust power of our coaxial system. As the rotor planes are sufficiently close together, we consider them as only one disk-plane as is depicted in Figure 2.2 and for a first approach we

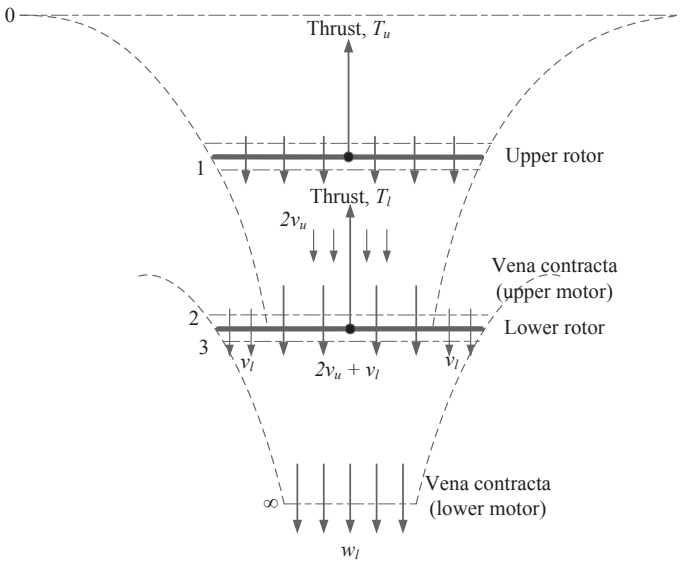

Figure 2.3: Flow model of a coaxial rotor system with the lower rotor operating in the slipstream of the upper rotor.

take into account that each rotor provides an equal fraction of total system thrust $W = 2T$ where $T_u = T_l = T$, which means that we can treat the coaxial system as a single rotor system. Thus from (2.6) and (2.7), we can see the effective induced velocity v_i and the induced power $P_{i_{coax}}$ for a dual rotor system as follows

$$v_{i_e} = \sqrt{\frac{2T}{2\rho A}} = \sqrt{\frac{T}{\rho A}} = \sqrt{\frac{W}{2\rho A}} \tag{2.8}$$

$$P_{i_{coax}} = 2Tv_{i_e} = 2T\sqrt{\frac{2T}{2\rho A}} = \frac{(2T)^{\frac{3}{2}}}{\sqrt{2\rho A}} = \frac{2\sqrt{2}T^{\frac{3}{2}}}{\sqrt{2\rho A}} \tag{2.9}$$

Consider that each rotor operates in an isolated way. The following scenarios are consider. Only one motor is operating, therefore the induced power is a half of $P_{i_{coax}}$. From (2.7) induced power for either rotor will be Tv_i, from the consideration

that

$$W = 2T \tag{2.10}$$

and the induced power for an isolated motor of a coaxial system is given as

$$P_{i_{isolated}} = 2Tv_i = 2T\frac{\sqrt{T}}{\sqrt{2\rho A}} = \frac{2T^{\frac{3}{2}}}{\sqrt{2\rho A}} \tag{2.11}$$

Comparing these results, a ratio between induced power for isolated rotor system (P_i) and the induced power for a dual rotor system (P_{coax}) is obtained. This is an interference-induced power factor k_{int} which is given by

$$k_{int} = \frac{P_{coax}}{P_i} = \left(\frac{2\sqrt{2}T^{\frac{3}{2}}}{\sqrt{2\rho A}}\right)\left(\frac{2T^{\frac{3}{2}}}{\sqrt{2\rho A}}\right)^{-1} = \sqrt{2} \tag{2.12}$$

Then, the induced power of a coaxial system could be written as

$$(P_i)_{coax} = k_{int}\frac{(2T)^{\frac{3}{2}}}{\sqrt{2\rho A}} = k_{int}\frac{W^{\frac{3}{2}}}{\sqrt{2\rho A}} \tag{2.13}$$

Notice that the net slipstream velocity w is produced by a coaxial rotor relative to two equivalent single rotor systems of the same radius generating the same thrust. In the ideal case, the wake will contract to a value that is half of the disk area, so from considerations for the coaxial system $w = 2v_{i_e}$. Because v_{i_e} is $\sqrt{2}$ higher than the induced velocity found with the two single rotors under the present assumptions, the slipstream velocity of the coaxial is then a factor $2\sqrt{2}/2 = 1.41$. This means that to achieve the same downwash velocities, a coaxial rotor operated at a lower effective disk loading than a single rotor machine when carrying the

same weight [62].

In practice, the two rotors of a coaxial system are never operated at the same thrust, but at whatever individual thrust level, is necessary to give a balance (equal and opposite) torque on the two rotors as a system. This is because both of the rotors share the same value of induced velocity, so that $P_u = P_l = P$ where

$$P_u = T_u v_{i_e} = T\sqrt{\frac{2T}{2\rho A}} \tag{2.14}$$

$$P_l = T_l v_{i_e} = T\sqrt{\frac{2T}{2\rho A}} \tag{2.15}$$

This means that for a coaxial rotor system with the rotors in the same plane operated at either the same thrust and/or the same torque, there exist a interference factor $k_{int} = 1.414$. Notice that in the case where the rotors operate in the same plane, a torque balance can be achieved only if the equality $Tu = Tl$ holds; other variations of thrust sharing will spoil the torque balance. In this way, recalling (2.11) and (2.8) it follows that

$$W = \frac{k_{int} P_i}{v_{i_e}} = \frac{1.41(2T)^{\frac{3}{2}}}{\sqrt{2T}} = 1.41T \tag{2.16}$$

in which A is tha area of the proppeller's disk and ρ the air density.

2.4 Forces and Moments Interacting in the Coaxial Heliciopter

Besides the thrust force, there are lateral forces and torques generated by the interaction between the control surfaces and the wind generated by the propellers. This is described below.

For the sake of simplicity, the velocity v_i can be thought to be perpendicular to the propeller disk, i.e. aligned with the body z-axis (see Figure 2.5). As the blades of the coaxial motor rotate, they are subject to drag forces around the aerodynamic center. This moments act in opposite direction relative to their angular velocity. In hover, the reactive torque generated in free air by the rotor is given by

$$Q_i \;\; = \;\; k\omega_i, \;\; k = 1, 2 \tag{2.17}$$

By considering each control vane as a wing immersed into a relative wind, the aerodynamic lift and drag forces, L and D, can be computed as

$$L = \tfrac{1}{2}\rho A_S C_L v_i^2 \quad , \quad D = \tfrac{1}{2}\rho A_S C_D v_i^2 \tag{2.18}$$

where A_S is the vane's surface and C_L, C_D are, respectively, the lift and drag coefficients (see also Figure 2.5). For reasonably small angles of attack α, it turns out that

$$C_L = c_L\alpha \quad , \quad C_D = c_D\alpha^2 + c_{D_0} \tag{2.19}$$

with C_L, C_D constant parameters which depend on the airfoil profile (which in this case is the same for all the control surfaces) and on the vane's angle of attack. The steering system is composed of two independent control vanes, whose angles of attack are denoted, respectively, by a and b (shown in Figure 2.5). By construction, the resultant lift forces denoted by F_L^x and F_L^y are directed along the body axes of the vehicle x and y, respectively, and their points of applications form with respect to the vehicle center of mass (CM) and a lever arm of length d shown in Figure 2.4. In this way two torques are generated to control the roll and pitch angles.

In summary, by considering the contributions of the control vanes of the propeller, the forces and torques that govern the system dynamics are given by

$$f^b = \begin{bmatrix} F_L^x \\ F_L^y \\ -W + F_D \end{bmatrix} + R^T \begin{bmatrix} 0 \\ 0 \\ Mg \end{bmatrix} \quad , \quad \tau^b = \begin{bmatrix} -F_L^x d \\ F_L^y d \\ Q_1 - Q_2 \end{bmatrix} + R^T \begin{bmatrix} 0 \\ 0 \\ Mg \end{bmatrix} \tag{2.20}$$

knowing that

$$F_L^x = \tfrac{1}{2}\rho c_L A_S a v_i^2 \quad , \quad F_L^y = \tfrac{1}{2}\rho c_L A_S b v_i^2 \tag{2.21}$$

where g is the gravity acceleration and F_D denotes the sum of all the drag forces of the control vanes in both levels which can be obtained by using equations (2.18) and (2.19).

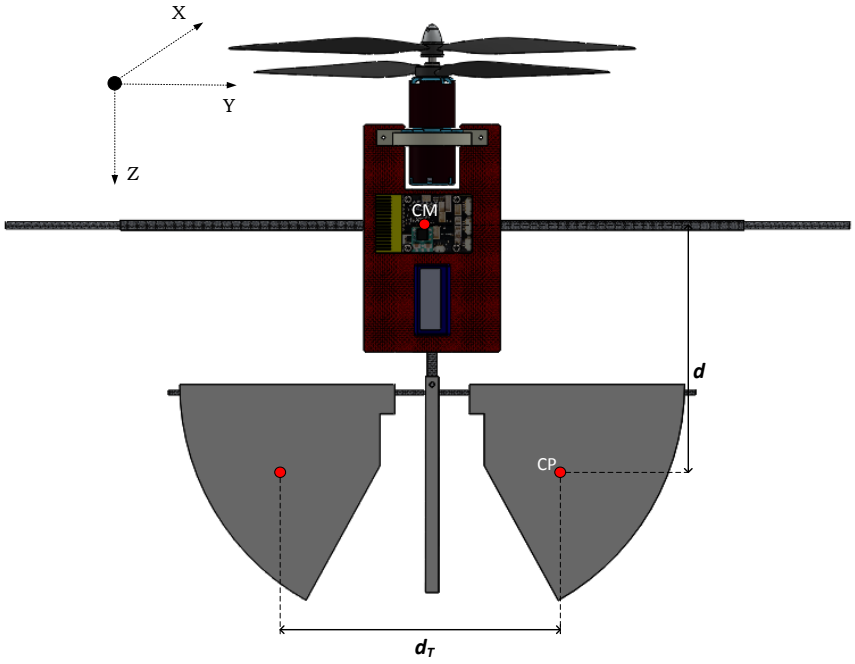

Figure 2.4: Lateral view of the coaxial helicopter showing the distance separation between the center of mass and pressure, and the distance separation d_T between the vane's pressure center.

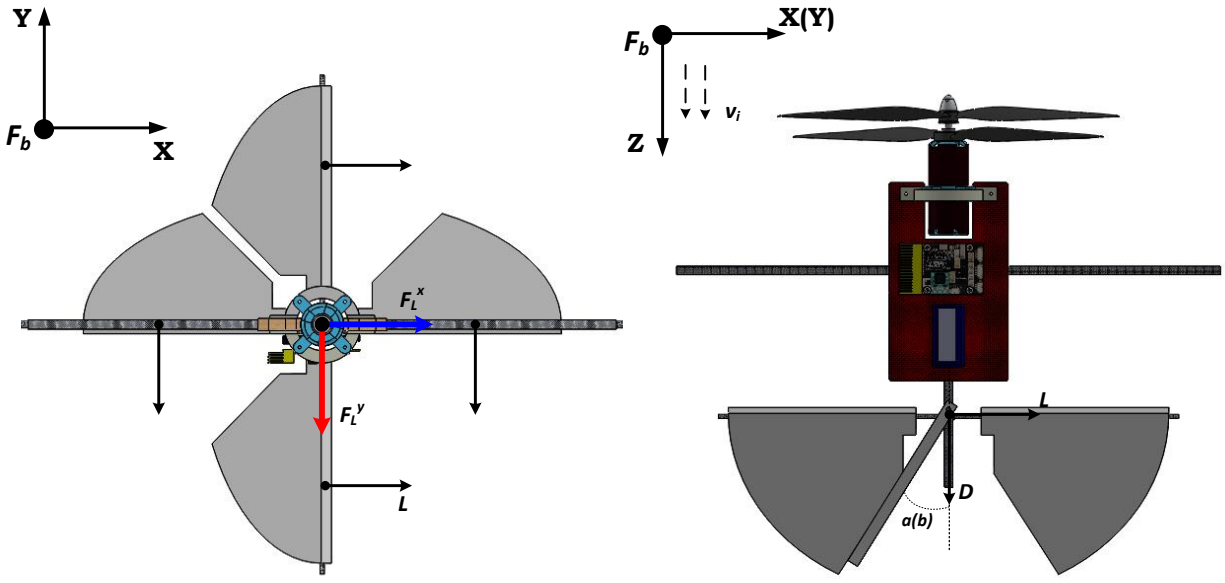

Figure 2.5: Aerodynamical forces and moments generated by the control surfaces.

3

Control Strategy

In this chapter, a bounded Lyapunov-based control law developed on the special orthogonal group is presented to steer a coaxial mini aerial vehicle (MAV) along a desired rotational maneuver. The proposed controller overcomes the singularities and ambiguities that some other control techniques have in several strategies in the literature. The key idea behind the proposed strategy, is to use the non-lineal manifolds to representate the rotational motion of the vehicle and also use bounden inputs taking into account the physical saturation limits of the actuators. For this purpose, a nested saturation control is proposed. The resulting control strategy yields global convergence of the current rotational maneuver.

Contents

3.1 Introduction

The attitude control problem has been extensively studied under various assumptions, but since some of these controllers are based on Euler angles [44] or quaternions [46], they exhibit singularities when representing complex rotational maneuvers of a MAV or it could be present ambiguities, thereby fundamentally restricting their ability to track non-trivial trajectories.

Most of the prior work on the attitude control for aerial vehicles is based on unit quaternions and three-parameter representations of attitude. Quaternions determine any point on the sphere and are redundant as the two poles of the sphere correspond to the same physical posture of the body, i.e. they account for two equilibria, which brings especial difficulties to the stability analysis of the attitude-controlled rigid bodies [63]. On the other hand three-parameter representations of attitude introduces an additional level of complexity to the control law, in addition singularities of attitude representation are presented in this kind of attitude representation, which complicates path planning and can seriously constrain admissible attitudes [64].

Linear control systems such as proportional derivative controllers or linear quadratic regulators (LQR) are widely used to enhance the stability properties of an equilibrium [65], [66], [67], [68]. A nonlinear controller is developed for the linearized dynamics of a quadrotor UAV with saturated positions in [69] [70].

In this thesis a geometric control technique in combination with a nested saturation algorithm is developed in order to completely avoid singularities that are associated with local coordinates and to analyze controllers that can achieve complex aerobatic maneuvers for a coaxial MAV. The dynamics of the MAV are expressed globally on the configuration manifold, which is the special orthogonal group $\mathsf{SO(3)}$. Moreover, the nested saturation part allows to get bounded controllers. The controller developed in this paper uses a configuration error function on $\mathsf{SO(3)}$ proposed in [71], which permits a good tracking performance uniformly in large initial attitude errors in contrast to the classical configuration error function studied in [48], [51], [72]. Also, The proposed controller exhibits the following unique features: (i) It guarantees almost global tracking features of the MAV as the region of attraction almost covers the attitude configuration space $\mathcal{SO}(\ni)$. Therefore, aggressive maneuvers of a MAV can be achieved in a unified way, without need for complex reachability analyses. (ii) It is coordinate-free. Therefore, it completely avoids singularities, complexities, discontinuities, or ambiguities that arise when using local coordinates or quaternions.

3.2 Attitude Tracking Control

In this section an attitude control strategy for stabilization of the the attitude dynamics (last two eqs. of (2.1)) of the *LaBola* aerial robot is developed.

Let's define the following configuration error function, the angular velocity error

vector and the attitude error vector inspired in [71] which are stated in the following

Proposition 1. *For a given tracking command (R_d, Ω_d), and current attitude and angular velocity (R, Ω), we define an attitude error function $\Psi : \mathsf{SO(3)} \times \mathsf{SO(3)} \to \mathbb{R}$, an attitude error vector $e_R : \mathsf{SO(3)} \times \mathsf{SO(3)} \to \mathbb{R}^3$, and an angular velocity error vector $e_\Omega : \mathsf{SO(3)} \times \mathbb{R}^3 \times \mathsf{SO(3)} \times \mathbb{R}^3 \to \mathbb{R}^3$ as follows*

$$\Psi(R, R_d) = 2 - \sqrt{1 + \mathrm{tr}[R_d^\intercal R]}, \tag{3.1}$$

$$e_r(R, R_d) = \frac{1}{2\sqrt{1 + \mathrm{tr}[R_d^\intercal R]}} (R_d^\intercal R - R^\intercal R_d)^\vee, \tag{3.2}$$

$$e_\Omega(R, \Omega, R_d, \Omega_d) = \Omega - R_d^\intercal \Omega_d. \tag{3.3}$$

For a fixed R_d, the attitude error function Ψ can be considered as a function of R only. The attitude error vector e_R is well defined in the sublevel set $L_2 = \{R \in \mathsf{SO(3)} \mid \Psi(R, R_d) < 2\}$. Then, the following statements hold.

(i) Ψ is positive definite about $R = R_d$.

(ii) in L_2, the left-trivialized derivative of Ψ is given by

$$T_I^* L_R(\boldsymbol{D}_R \Psi(R, R_d)) = e_R. \tag{3.4}$$

(iii) in L_2, the critical point of Ψ is $R = R_d$.

(iv) in L_2, Ψ is locally quadratic, i.e.,

$$\|e_R\| \leq \Psi(R, R_d) \leq 2 \|e_R\|^2 . \tag{3.5}$$

(v) in L_2, e_R is bounded such that

$$\|e_R\| \leq 1. \tag{3.6}$$

Proof. The proof can be seen in [71]. □

3.2.1 Attitude Error Dynamics

The attitude error dynamics of the for the attitude error function ψ, the attitude error vector e_R and the angular velocity error vector e_Ω is given in the following

Proposition 2. *In L_2, the error dynamics for Ψ, e_R, and e_Ω satisfies*

$$\frac{d}{dt}(\Psi(R, R_d)) = e_R \cdot e_\Omega, \tag{3.7}$$

$$\|\dot{e}_R\| \leq \frac{1}{2}\|\dot{e}_\Omega\|, \tag{3.8}$$

$$\dot{e}_R = E(R, R_d), \tag{3.9}$$

$$\dot{e}_\Omega = J^{-1}(-\Omega \times J\Omega + \tau_b) + \hat{\Omega}R^\intercal R_d\Omega_d - R^\intercal R_d\dot{\Omega}_d. \tag{3.10}$$

where $E(R, R_d)$ is given by

$$E(R, R_d) = \frac{(\mathrm{tr}[R^\intercal R_d]I - R^\intercal R_d + 2e_R e_R^\intercal)}{2\sqrt{1 + \mathrm{tr}[R_d^\intercal R]}}e_\Omega \tag{3.11}$$

Proof. The proof can be seen in [73]. □

3.2.2 Attitude Tracking Control for *LaBola*

It is important to notice that the control approach should take into account the fact that in real applications the thrust is by nature non-negative and is generated by actuators having saturation limits. This motivates us to define the controllers in terms of linear saturation functions, whose definition is given next.

Definition 1. *Given two positive constants L, M with $L \leq M$, a function $\sigma : \mathbb{R} \to \mathbb{R}$ is said to be a* linear saturation *for (L, M) if it is a continuous, non-decreasing function satisfying:*

a) $s\sigma(s) > 0$ for all $s \neq 0$;

b) $\sigma(s) = s$ when $|s| \leq L$;

c) $|\sigma(s)| \leq M$ for all $s \in \mathbb{R}$.

The main result is summarized in the following theorem.

Theorem 3. *Suppose that a smooth attitude command $R_d(t)$ satisfying $\dot{R}_d = R_d\hat{\Omega}_d$ is given. Let $K_R, K_\Omega \in \mathbb{R}$, (L_{e_R}, M_{e_R}), $(L_{e_\Omega}, M_{e_\Omega})$ be positive constants, where $M_{e_R} < \frac{1}{2}L_{e_\Omega}$ holds. Consider linear saturation functions σ_{e_Ω} and σ_{e_R}. Then, the control input $\tau^b \in \mathbb{R}^3$ given by*

$$\begin{aligned} \tau^b &= -\sigma_{e_\Omega}(K_\Omega e_\Omega + \sigma_{e_R}(K_R e_R)) + \Omega \times J\Omega \\ &\quad -J(\hat{\Omega}R^\intercal R_d\Omega_d - R^\intercal R_d\dot{\Omega}_d) \end{aligned} \tag{3.12}$$

stabilizes the zero equilibrium of the tracking error (e_R, e_Ω) *exponentially.*

Proof. In order to prove exponential stability, consider the following candidate Lyapunov function

$$W = \frac{1}{2} e_\Omega^\intercal J e_\Omega + K_R \psi(R, R_d) + c_2 e_\Omega^\intercal e_R \tag{3.13}$$

for a positive constant c_2. Furthermore, the time-derivative of W along the trajectories of the closed-loop system of Proposition 2 and (3.12) is given by

$$\begin{aligned} \dot{W} &= e_\Omega^\intercal J \dot{e}_\Omega + K_R \dot{\psi} \\ &= e_\Omega^\intercal \left[-\sigma_{e_\Omega}(K_\Omega e_\Omega + \sigma_{e_R}(K_R e_R)) \right] + K_R e_R^\intercal e_\Omega \\ &\quad + c_2 e_R^\intercal \left\{ J^{-1} \left[-\sigma_{e_\Omega}(K_\Omega e_\Omega + \sigma_{e_R}(K_R e_R)) \right] \right\} \\ &\quad + c_2 e_\Omega^\intercal \dot{e}_R \end{aligned} \tag{3.14}$$

In order to analyze the first therm of the RHS of (3.14), consider the ideas taken from [74] and [75]. The analysis starts by considering the evolution of the state e_Ω. Given that $M_{e_R} < \frac{1}{2} L_{e_\Omega}$, it follows that $e_\Omega^\intercal J \dot{e}_\Omega < 0$, $\forall e_\Omega \notin Q_{e_\Omega}$ where $Q_{e_\Omega} = \{e_\Omega : K_\Omega |e_\Omega| \leq \frac{1}{2} L_{e_\Omega}\}$. As a consequence, e_Ω enters in the set Q_{e_Ω} in a finite time and remains in Q_{e_Ω} thereafter. Regarding state e_R, observe that once e_Ω has entered in the set Q_{e_Ω}, the argument of σ_{e_Ω} is bounded as $|K_\Omega e_\Omega + \sigma_{e_R}(K_R e_R)| \leq L_{e_\Omega} + M_{e_R} \leq L_{e_\Omega}$. Consequently, σ_{e_Ω} operates in its linear region after e_Ω has entered Q_{e_Ω}. Following the same procedure as for e_Ω it is possible to show that e_R enters an analogous set Q_{e_R} in finite time, and remains in Q_{e_R} thereafter. Taking into consideration the aforementioned discussion and (3.6),

(3.8), the time derivative of the candidate Lyapunov function (3.13) is bounded as follows

$$\begin{aligned} \dot{W} &\leq -\left(k_\Omega - \tfrac{c_2}{2}\right)\|e_\Omega\|^2 - \tfrac{c_2 K_R}{\lambda_{max}(J)}\|e_R\|^2 \\ &\quad -\tfrac{c_2 K_\Omega}{\lambda_{min}(J)}\|e_R\|\,\|e_\Omega\| \\ &= -z^\intercal W_2 z \end{aligned} \tag{3.15}$$

where $z = [\|e_R\|\,;\|e_\Omega\|] \in \mathbb{R}^2$ and $W_2 \in \mathbb{R}^{2\times 2}$ given as follows

$$W_2 = \begin{pmatrix} \frac{c_2 K_R}{\lambda_{max}(J)} & -\frac{c_2 K_\Omega}{2\lambda_{min}(J)} \\ -\frac{c_2 K_\Omega}{2\lambda_{min}(J)} & K_\Omega - \frac{c_2}{2} \end{pmatrix} \tag{3.16}$$

Parameters c_2, K_R, K_Ω can be chosen in order to the matrix W_2 become positive definite and then obtain exponential stability of the zero equilibrium of the attitude and angular velocity tracking error e_R, e_Ω.

□

4

Simulations and Experimental Results

This Chapter, simulations are derived and presented to demonstrate the effectiveness of the control law proposed on the above Chapter. Also, some experimental test made in real time with the experimental platform LaBola are described in order to corroborate the functionality of the platform.

Contents

4.1 Simulations and Experimental Results on *LaBola*

Several series of simulation has been performed to evaluate the controller of Chapter 3. The simulations are performed in Simulink^{TM} using a fixed-step size of 1×10^{-2} with Dormand-Prince solver. In the simulation settings the moments of inertia of the rigid body are $J = diag[3, 2, 1]kgm^2$ the initial conditions of the rigid body had chosen as follows:

$$R(0) = I, \qquad \Omega = [0, 0, 0]rad/s$$

The desired attitude command is described by using $R_d = R_d(\psi(t))R_d(\theta(t))R_d(\phi(t))$ and this angles are chosen as

$$\phi(t) = \theta(t) = \psi(t) = sin(2\pi ft)$$

generating a sinusoidal movement for the three angles in radians at a frequency $f = 2$ Hz, when the simulation time t is in seconds. The desired angle rates Ω_d are obtained from $\dot{R}_d = R_d\hat{\Omega}_d$. We have used the following linear saturation functions

for the error vectors

$$\sigma_{ij}(s) = \begin{cases} \frac{\arctan(a[s-L_{ij}])}{a} + L_{ij} & \text{if } s > L_{ij} \\ s & \text{if } |s| \leq L_{ij} \\ \frac{\arctan(a[s+L_{ij}])}{a} - L_{ij} & \text{if } s < -L_{ij}. \end{cases}$$

where $a := \frac{\pi}{2(M_{ij}-L_{ij})}$, with $M_{ij} > L_{ij} > 0$. Details about these saturation function such as its first and second time derivatives can be seen in [76].

The controller gains are chosen as $k_R = 5500$, $k_\Omega = 550$ and the saturations bounds are given by selecting $M_{e_R} = 700$. Simulations results are depicted in Figures 4.1 - 4.2. Furthermore, Figure 4.3 shows an image of the MAV in the experimental area during the real-time tests. In addition, a video showing *LaBola* experimental platform performing some experiments can be observed at `https://www.youtube.com/watch?v=QSxHX-HUuhU`.

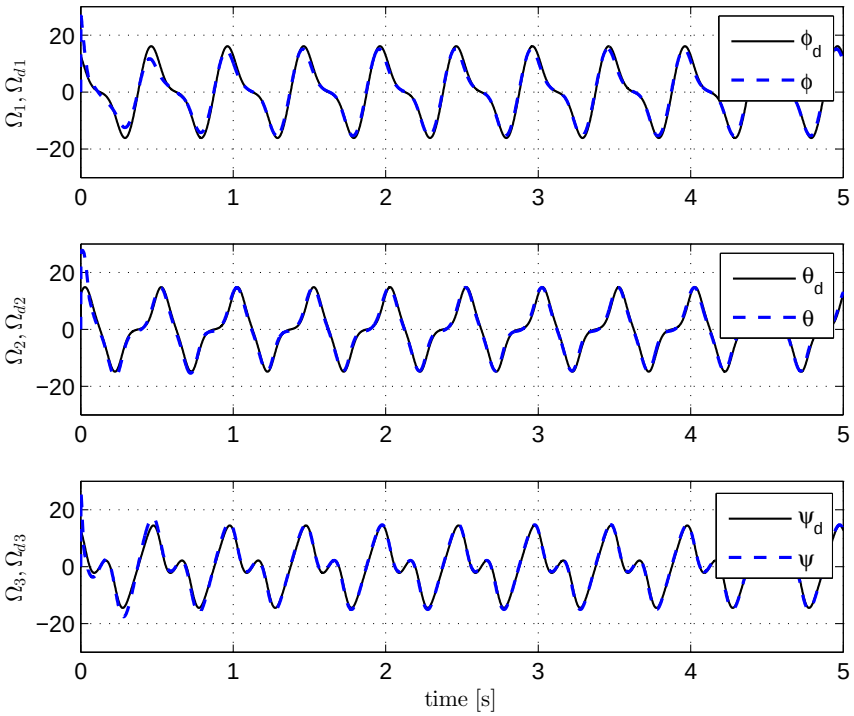

(a) Angular velocity Ω (rad/s).

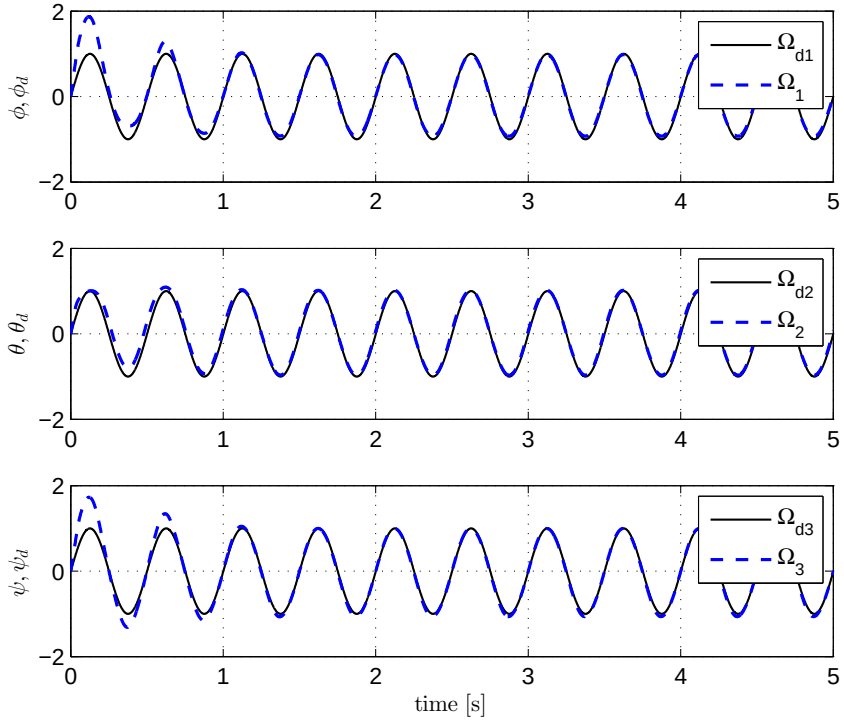

(b) Euler angles ϕ,θ,ψ (rad).

Figure 4.1: Attitude tracking (Proposed controller: blue, dashed; Desired command: black, solid).

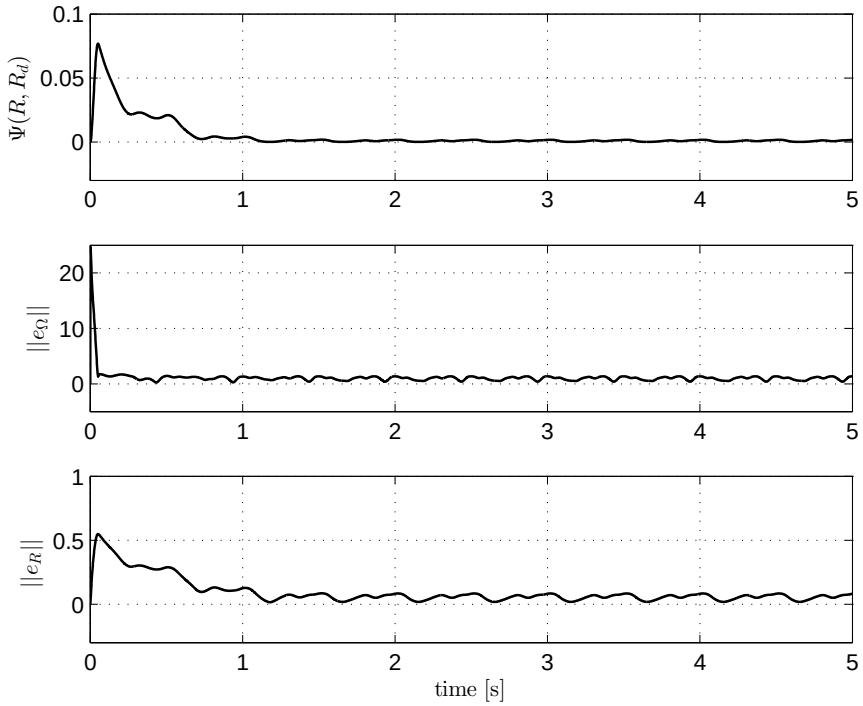

(a) Attitude error function Ψ, Magnitud of the angular velocity error $\|e_\Omega\|$ (rad/s) and the Magnitud of the rotational error $\|e_R\|$ (rad/s).

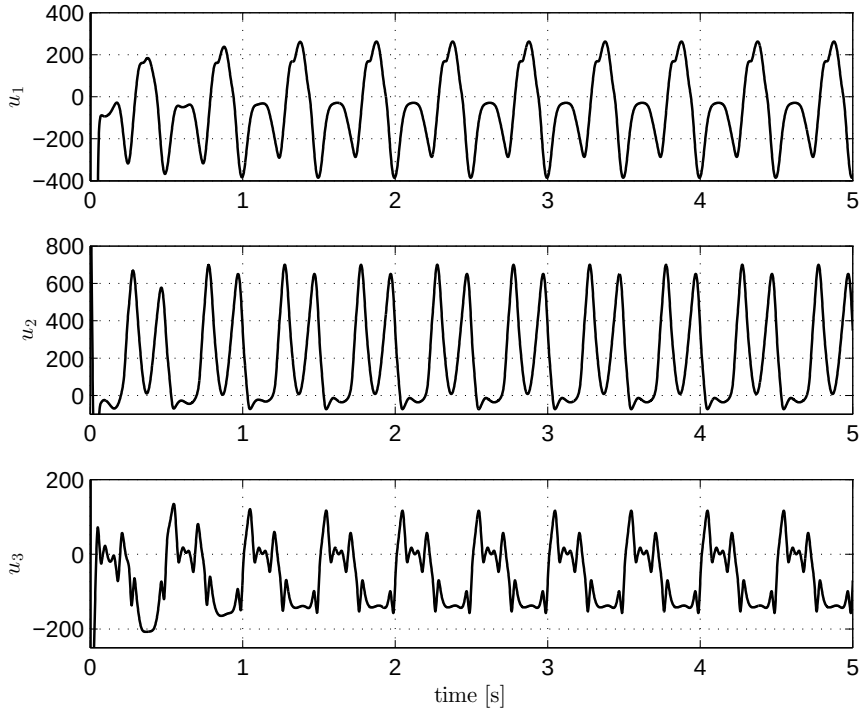

(b) Control inputs u (Nm).

Figure 4.2: The tracking error magnitudes and the control input signals.

Figure 4.3: *LaBola* aerial robot flying in the experimental area during real-time tests.

5

Experimental Platform

In this Chapter, the whole design process of the coaxial helicopter and its protection, the gimbal system, is presented. From a first planning stage, trough the materials selection, to the construction of the two experimental prototypes used in this thesis. Also, in this chapter there is a section dedicated to mention the developed work done on the autopilot PX4 ant its sensors, as well as the importance of using such device.

Contents

5.1 Introduction

Helicopters have played a unique role in modern aviation. New generations of small and lighter aircrafts are being developed in the last few years. Helicopters can be classified in function of their price, size, power, capability, etc., but their performance is a function of the rotor configuration. A helicopter classification, introduction and historical background can be found in [27].

The motion of the helicopter could be controlled by a swash plate linked to the lower rotor, this swashplate changes the collective pitch and cyclic pitch of the rotor through servomotors [32, 34, 52] or by moving control surfaces that deviate the airflow generated by the coaxial rotor [29, 38, 39]. In this work the control by vanes was chosen in order to reduce the complexity and coupled dynamics that generate the swashplate. Despite the lost of energy due to the interference between rotors, a twin rotor in coaxial configuration has been chosen to generate the thrust force taking advantage of its compactness.

5.2 The Coaxial Helicopter

During this thesis, several models were designed for the purpose of having a planning stage and select the best way of distributing the elements, i.e., avionics,

propulsion system, battery, etc., aboard the drone. The first platform drawn was intended to make it small (see Figure 5.2a.), this would help to reduce the based-gimbal protection size. Unfortunately this reduced design did not include the size and weight of the battery, this fact was reflected in the first built prototype: *ElCoaxial* which is depicted in Figure 5.1. Taking into account the shortcomings

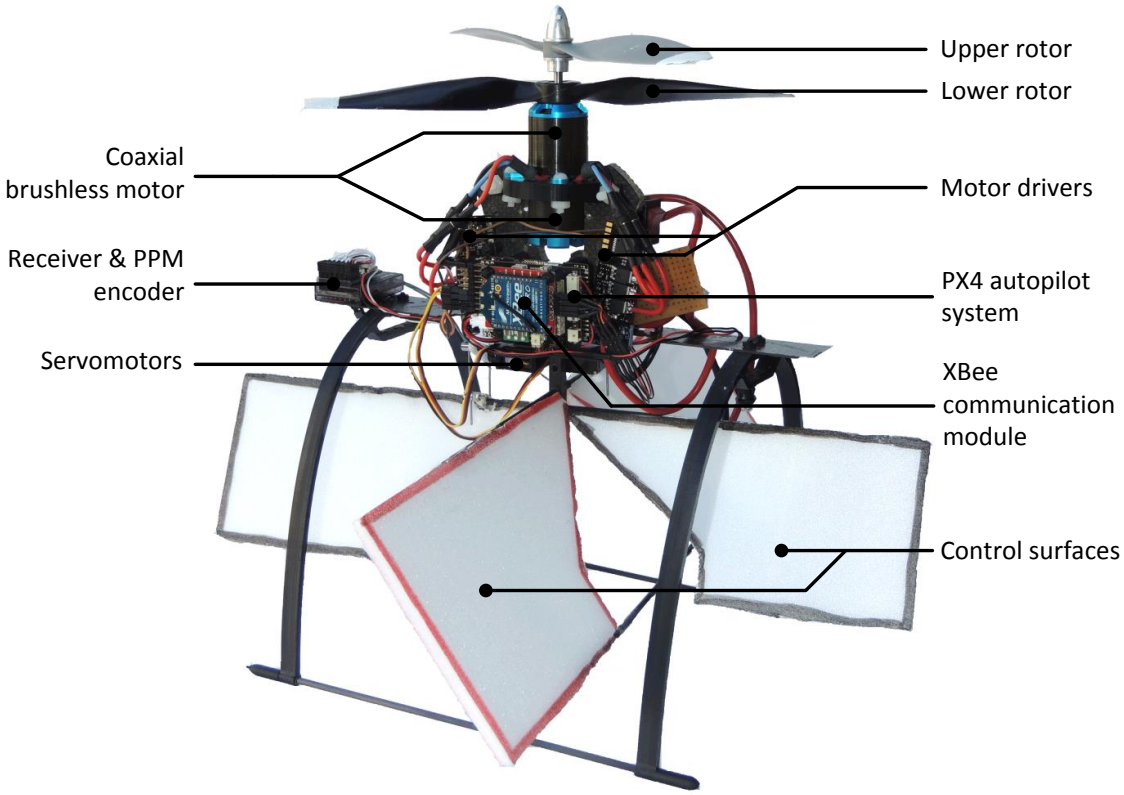

Figure 5.1: *ElCoaxial* first built experimental platform and its on-board elements.

of the first prototype, a second stage design was carried out sacrificing its small size, but considering and using the size and weight of the battery, i.e., using the battery weight to balance the vehicle center of mass. Within four proposed designs

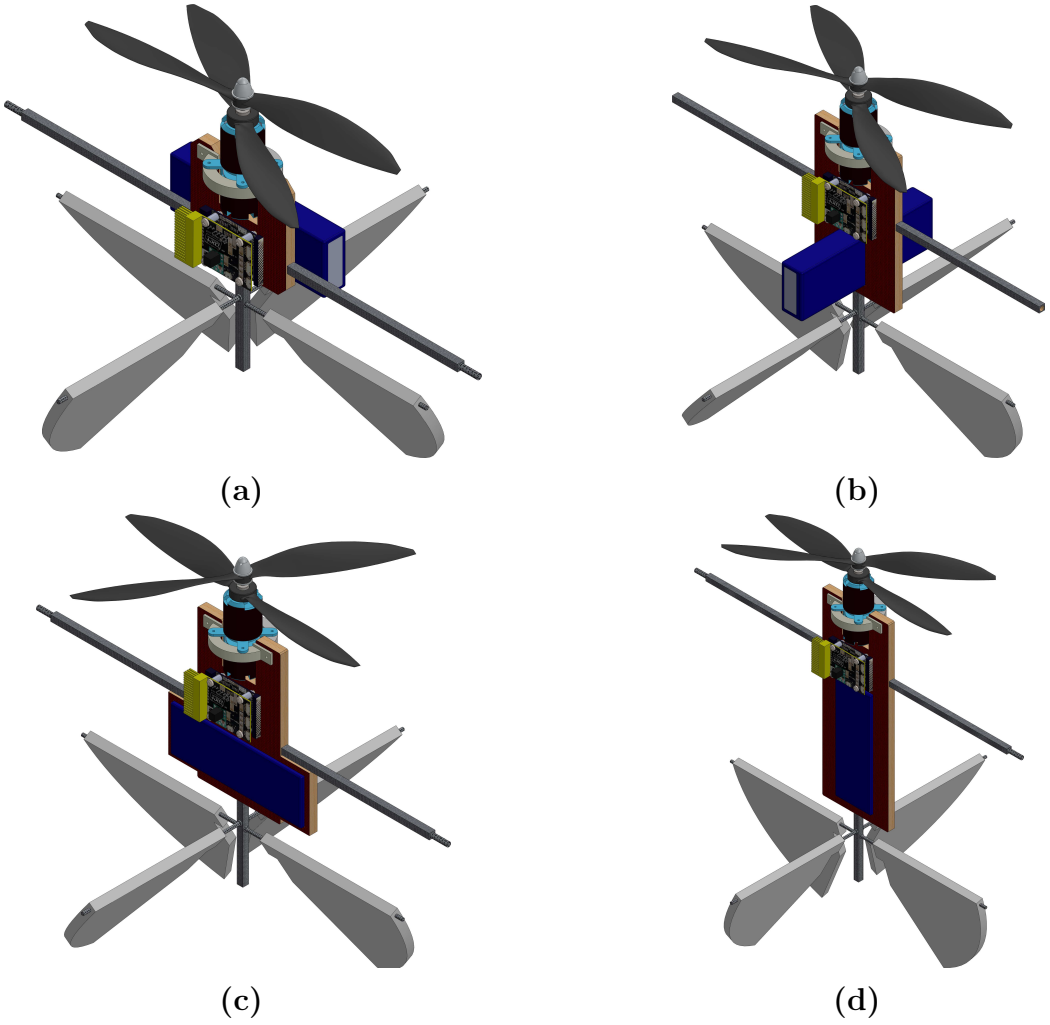

Figure 5.2: 3D CAD models of the novel coaxial aerial robot.

(depicted in Figure 5.2), the model shown in Figure 5.2b was chosen. The model selected shows that the interference with the air flow produced by the rotor is minimal and it does not compromise the rigidity of the main structure as the designs in Figures 5.2c and 5.2d, respectively. The selected design was also build and it could be see in Figure 5.3. The first MAV is 254 mm wing spam, 300 mm in height and has a total mass approximately of 650 g while the second prototype is 370 mm in height and a extra weight of 50 g. A specific distribution of weight is

Figure 5.3: Second built experimental platform: *LaBola* inner frame.

shown in tables 5.1a and 5.1b.

In both experimental platforms, the main frame holding the motor, the avionics, the servomotors and the battery are attached to a sandwich made of carbon fiber and balsa wood. The control vanes are made of depron for the first prototype while for the second, are made of balsa wood. The propulsion system is composed of a CR2816 Himax® contra-rotating coaxial brushless motor using the recommended propellers by the manufacturer and two Mikrokopter® electronic speed controllers (ESC) that are suitable to operate the twin motors. More information about features, specifications, and operation of the coaxial motor can be see in [77].
The architecture of the coaxial motor is exploited since it allows to overcome the gyroscope effect, control the yaw angle by a deferential speed variation between

(a) *ElCoaxial* frame

Element	Weight (g)
Battery	222
Coaxial motor	164
ElCoaxial Frame	144
Avionics	100
Servomotors	20
TOTAL	650

(b) *LaBola* inner frame

Element	Weight (g)
Battery	222
Coaxial motor	164
LaBola Inner Frame	194
Avionics	100
Servomotors	20
TOTAL	700

Table 5.1: The build platforms weight distribution.

the two rotors and control the altitude by varying the rotor speed.These vanes deviates the airflow coming from the the propellers creating a moment at the center of gravity allowing to tilt the vehicle. The electronic components of the vehicle including the avionics described in section 5.3, are powered by a 2800 mAh, 11.1 V lithium polymeer battery (LiPo). The vehicle and some of its components are depicted in Figure 5.3.

5.3 The PX4 Autopilot System Description

5.3.1 A Brief Introduction to Autopilots

Overtime, MAV platforms in research have been developed by using control systems to manage data sensors, output actuators, and in some cases weather information;

from micro-controllers as Rabbit [78] or DSP [32] to embedded computers as Gumstix [79].

The autopilot is a system used to help human operators to pilot a MAV; it allows the control of a vehicle by holding its attitude and position to make the task easier but without replacing the human control [80], i.e., the pilot has always the ability to take control of all variables (altitude, attitude and position). A very first use was seen in missiles during the World War II, after that, they were used on drones for target practice in 1930 and later [81]. However, these technology were developed only for large-scale Unmanned Aerial Vehicles (UAVs) but thanks to the development of computation technology, especially the microprocessor and MEMS inertial sensors, the small autopilots have become a hot research point in the field of the MAVs; an example of this is the autopilot based on DSP [82].

Nowadays, autopilots are used in a large variety of aircrafts, boats, multicopters, spacecrafts, etc., in order to track all the possible variables referring to the vehicle state or environment variables [83]. They can be purchased at almost any aeromodelling store where you could find autopilots from the most sophisticated to the simplest; in [84] is presented a brief survey of the autopilots used in the area of research. By now, newest autopilots not only can manage the position and attitude of the vehicle, but also can support missions like path following by integrating data from sensors like GPS, ultrasonic sensors, optical sensors, pressure sensors (barometric and pitot tube), temperature sensors and video transmissions, among others.

For this work a PX4 autopilot has been chosen to achieve the control of the vehicle

and manage data sensors. This flight stack is an electronic autopilot designed to control aircrafts, helicopters and multirotors from 4 to 8 rotors in its different configurations: "x", "+" or coaxial. Furthermore, this autopilot has been reached a big popularity due to its open-source support given by the PIXHAWK Project of the Computer Vision and Geometry Lab of ETH Zurich, by the Autonomous Systems Lab and the Automatic Control Laboratory [85] as well from a large number users.

5.3.2 Autopilot Hardware

The PX4 autopilot system is divided in two main parts: the Flight Management Unit (FMU) and the Input-Output (IO) modules which are depicted in Figure 5.4. The FMU can operate individually to stabilize a vehicle since it has a 68 MHz / 252 MIPS Cortex-M4F microprocessor and a 192KB SRAM / 1024 KB flash memory. In terms of communications protocols it has two modules I2C, 4 serial ports, a PPM port, a SPI port and a bus CAN. It is also useful to mention that it counts with 3 inertial sensors, and 4 PWM servo outputs. However, the IO board enhance the capability and protection of the FMU module by adding a 24 Mhz Cortex-M3 failsafe microcontroller enduring voltages from 7 to 17V wide supply and giving reverse polarity protection on all power inputs. Also the IO board adds 8 high-speed servo outputs up to 400 Hz PWM rate. The PX4 system has a stacking concept for combining the PX4FMU autopilot-on-module with a carrier board that interfaces any supported platform, also it provides a stable 5V power

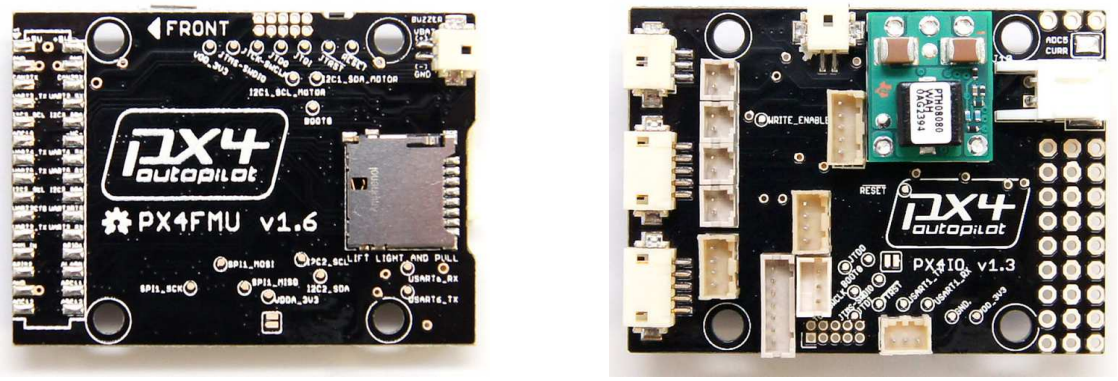

(a) A The FMU Board. **(b)** B The IO Board.

Figure 5.4: The PX4FMU Autopilot System: The FMU v1.6 (a) and its expansion, the IO board v1.3 (b).

supply. This concept allows customized solutions for different type of vehicles whilst still sharing the same autopilot module and sensors. Based on the above, the challenge and contribution in this work was to create a modified firmware which docked at characteristics of the experimental platform proposed in Section 5.2, i.e., create a firmware capable of combining coaxial helicopter actuators, sensors aboard PX4 fligh stack, partly using the original firmware programs which can be found in [86].

5.3.3 Supported Sensors

There are many sensors that are fully developed to use in cooperation with the PX4 system obtaining the vehicle position and attitude data and weather conditions of the flying area. The available sensors for the PX4 are:

- 3D Accelerometer / Gyro: MPU-6000

- 3D Gyro: L3GD20
- 3D Magnetometer: HMC5883L
- Barometric pressure: MS5611
- GPS receiver: 3DR uBlox LEA-6H
- Ultrasonic sensor or SONAR: HRLV-MaxSonar-EZ (MB1043)
- Image sensors: 752x480 MT9V034
- Airspeed sensor: 4525DO

The control of a vehicle in attitude and position and the performing of specific missions requires the cooperation between different subsystems. All the sensors mentioned above joined with the PX4 autopilot system (software and hardware) comprise the avionics of the vehicle. The LiPo battery and the electronic speed controllers (ESC) conform the power system. The communication system is conformed by the radio controller (RC), the ground control station (GCS) and the on-board receivers. Figure 5.5 shows a connection diagram of these subsystems.

5.3.4 Possible Configuration Sensor

Considering the sensors mentioned in subsection 5.3.3, it is possible to create combinations between them according to the MAV or the mission to perform. For example, a GPS u-blox module shown in Figure 5.6a, the ultrasonic sensor with the image sensor (both assembled in PX4FLOW, depicted in Figure 5.6b) and the

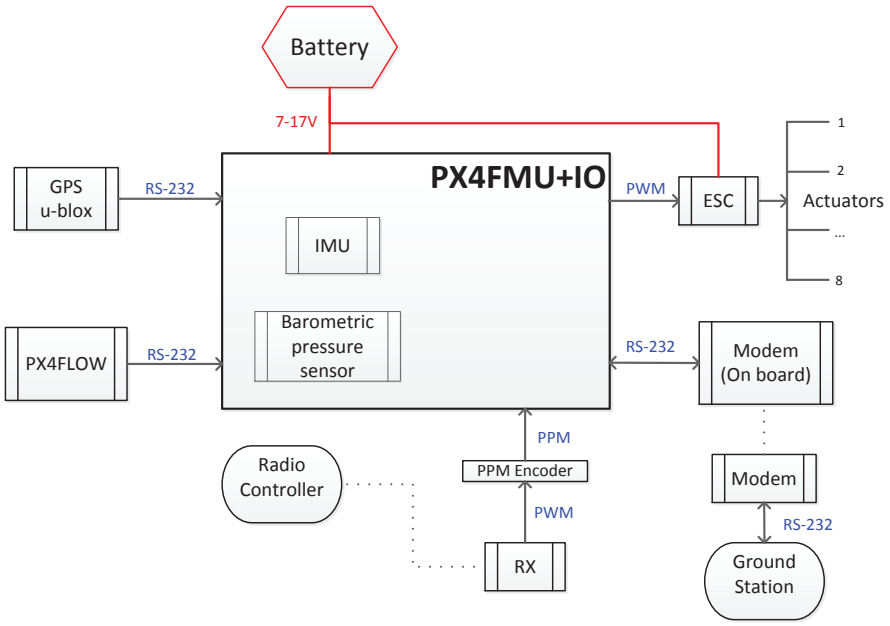

Figure 5.5: The PX4FMU hardware framework: Sensors, power and communication subsystems.

inertial sensors mounted on the PX4FMU. This configuration could be used in order to have extra data and achieve the vehicle control in position and attitude through the PX4 specific applications which integrate this data sensors send it to the actuators. The most important PX4 sensors combination are described as follows:

- **GPS Module and IMU:** GPS plays an important role in the autonomous control of MAVs, because it provides an absolute position measurement [84]. A known bounded error between GPS measurement and the real position can be guaranteed as long as there is a valid 3-D lock. For instance, u-blox 6 GPS receiver could achieve a two meter 3-D accuracy with the Satellite Based Augmentation System (SBAS). This first combination integrates data

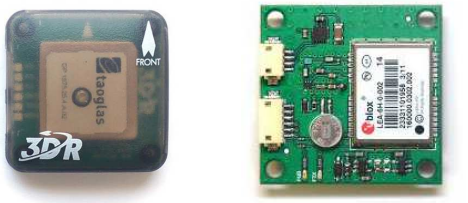

(a) GPS u-blox 6 module.

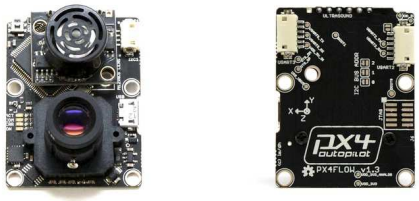

(b) The PX4FLOW board.

Figure 5.6: External sensors: The GPS u-blox 6h (a) and the PX4FLOW board v1.3 (b).

from default inertial sensors on the PX4FMU (Sensor Data) and the GPS information (Raw Data), after that, a position and attitude estimation is done by the PX4FMU. This interaction between the GPS module and the PX4 system can be seen in Figure 5.7.

- **PX4FLOW board and IMU:** In this combination the PX4FLOW board acts as a local GPS since it is possible know the position and velocities of the vehicle. Therefore another possible combination is integrating the PX4FLOW board information (Raw Data) and the inertial data coming from the PX4FMU board (Sensor Data) and then, as in the last configuration, it is possible to make an estimation and control of the position and attitude of the vehicle.

For this work, several experiments were conducted using the first combination (GPS + PX4FMU), these experiments were performed with *ElGuapo* quadrotor

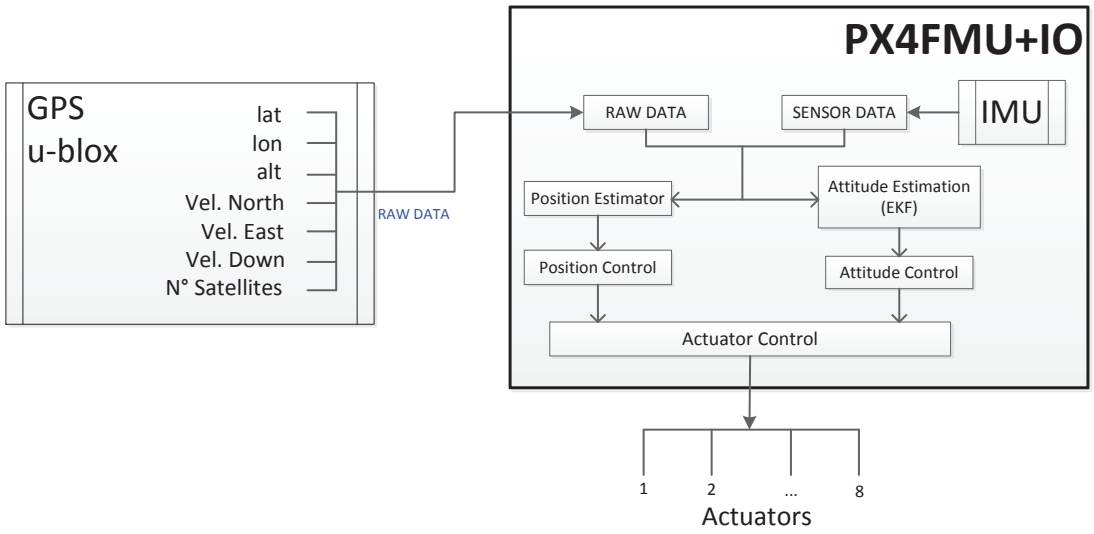

Figure 5.7: GPS with PX4 configuration.

[87] to achieve position control. This experiments were done to confirm the system operation under certain circumstances. The main objective is take advantage of the modularity of the PX4 system and add the GPS and the application which manages position control (see `mc_pos_control` in [86]) to the set of applications running in real time on the the new created platform for the coaxial vehicle *LaBola*. To see this experiments refers to section 6.3.

5.4 The Gimbal Protection

5.4.1 Elastic Protection Mechanisms

The prototypes based on propellers require a rigid internal structure as the aerodynamic depends on the geometric position of the rotors, the center of mass and / or control actuators, i.e., flight engines also must not be placed on flexible structures to prevent contact with other parts of the platform / user due to fast-spinning propeller. The main requirement of protective structures on a flying robot is thus to shield this frame, the sensitive components mounted on it and the spinning propellers from damage resulting from a collision.

Some aerial vehicles use rigid protective mechanisms attached to the main structure of the vehicle in order to absorb the energy generated in an impact leveraging the compression of matrial [88][89], but although these materials are resistant to low-energy impacts and has a simple design, the rigid protection transferred all the impact energy of a collision into the inner frame of the platform. As the absorption distance is minimal, strength in the structure quickly reaches high values and nothing beyond a beat at low speed can cause damage to the structure.

This is a particular problem that a flying robot faces in a crowded environment. In the case of carbon fiber, the most commonly materia used for platform structures,

the damage caused by collisions is directly related to the impact force on the structure and can cause extensive de-lamination and cracking [90]. A single collision is enough to reduce the residual strength of the material, making it more vulnerable to subsequent collisions [91]. In addition to the compressive forces on the structure, the impact force on a protective mechanism in rigid protection can cause high torques at its point of connection to the chassis of the robot. Some platforms minimize this damage by using "mechanical damping" such as nylon screws or rubber around the propeller which can be easily and quickly replaced. Despite all prevention to avoid costly damage, one impact still makes a platform unusable.

To consider an adequate protection from collisions, the assumption that a flying platform should survive an impact with a surface at a speed of 5 m/s was made. In order to survive the collisions a flying platform can encounter over its lifetime a protective structure must absorb all the energy of an impact while minimizing the force placed on the frame. Assuming that impact occurs with a stiff, inelastic surface, such as a concrete floor, the protective structure must mechanically absorb all the kinetic energy of the entire platform.

Considering the above, special attention have been paid in the design of a mechanisms for protecting the MAV frame. In order to endure collisions caused by for example, lack of sensor information, the main idea of this project is make a vehicle not only able to stay stable, but also to give extra protection to the user and the vehicle. This is achieved by adding a protector mechanism capable to minimize the friction caused by the impacts. A protective frame is decoupled from

the inner frame by means of a gimbal system, in that way, the protection has free movement in three degrees of freedom (DOF) while the helicopter remains stable inside the protection. The inner frame contains the conventional propulsion and stabilization systems described in section 5.2.

5.4.2 Protective Structure Design

The following steps were followed in the design of the gimball protection and are proposed to design and dimension elastic protective structures for flying platform:

1. **Protection Configuration:** Configuration on the platform should be selected to increase absorption distance, minimize force on the platform's structure and protect from impacts in the most likely directions.

2. **Material Selection:** A material should be chosen so that it has the required stiffness, yield strength and density to absorb the required energy.

3. **Dimensioning:** Individual elements should be optimized to minimize weight.

5.4.2.1 Proteccion Configuration

Considering the disadvantages of a rigid structure (see Section 5.4.1), it was decided to make a rigid structure but with the advantages of a gimbal system, i.e., movable in three axes to improve the resilience to collisions and to minimize the friction

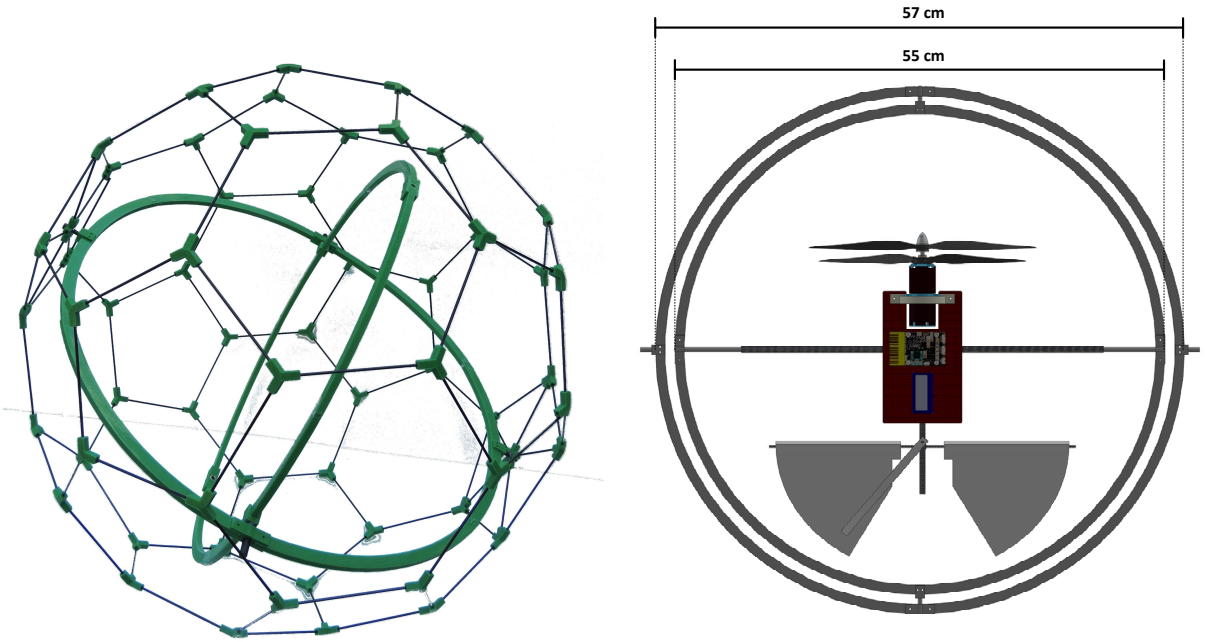

(a) Assembled gimbal protection.

(b) Dimensions of the two ABS circle protection.

Figure 5.8: The plastic and carbon fiber protection 5.8a and the real circles dimensions in the Solidworks® assembly 5.8b.

force between a protective frame and obstacles. Such protective structure is divided into 3 main parts: the first pieces are two printed circles ABS Plastic 57 cm and 52 cm (shown in Figure), respectively, and the second is a truncated icosahedron was chosen to make the external protection. This geometry associated with footballs (soccer balls) has 12 regular pentagonal faces, 20 regular hexagonal faces, 60 vertices and 90 edges (see Figure 5.8a). Note that even taking into account all these considerations is still very hard to achieve because protective frames cannot be designed to be perfectly smooth and prevent friction with all obstacles.

5.4.2.2 Material Selection

The geometry of the protection was not the unique problem, also the material to make it has an important roll since the final weight of the prototype and also the stiffness and strength are engaged. The material used for the external protection should absorb the largest amount of energy without breaking at the lowest weight. Then, three factors that must be considered are:

- The materials stiffness defined by its Young's modulus E. This parameter means that at a higher stiffness, the material absorbs more energy.
- The tensile yield strength μ which indicates that at a higher strength the material resists plastic deformation.
- The density ρ that shows that lower density yields lower weight.

Some important material properties can be seen in Table 5.4.2.2[i]. The material most adapted for use in flying robots due to their high compression strength and stiffness [92] and low cost is carbon-fiber reinforced plastic (or simply carbon fiber), as it has almost the same stiffness E than the stiffest metals (Brass, Stainless Steel and Titanium alloy). The values available in literature are approximative values, as they vary greatly depending on samples and testing methods. It is even more variable with composite materials as it depends on thread size, weaving pattern, percentage of fiber to plastic, type of plastic and weave direction [25].

[i]The material data was tooked from `http://www.matweb.com/`

Material	Young's modulus E $[GPa]$	Tensile Yield Strength μ $[MPa]$	Density ρ $[g/cm^3]$
Rubber	0.055 +/− 0.045	8	1.055 +/− 0.145
Nylon	3.0 +/− 1	78	1.13
Brass	112.5 +/− 12.5	247	8.560 +/− 0.165
Aluminum	69	275 +/− 35	2.7 +/− 0.165
Stainless Steel	200	600	7.900 +/− 0.150 25.32
Titanium alloy	112.5 +/− 7.5	977	4.510
Glass-fiber	31.65 +/− 14.45	1500	1.8
Aramid	70.5	2757	1.44
Diamond	1220	2800	3.530
Carbon-fiber	135 +/− 15	2000	1.570
ABS plastic	1.7	55	1.38

Table 5.2: Selected Material properties.

Due to the special configuration of the vertices and the properties of the materials mentioned above, the vertices, joints and arcs were printed in ABS plastic with 3D printer and the edges of the protection are made of 2mm carbon fiber tubes of 9 cm large. Therefore, ball bearings of 4 mm of diameter were used in the joints to minimize the friction. The weigth of each part of the gimbal system protection as the total weight is specified on table 5.4.2.2.

Element		Weight (g)
Plastic union	× 60	120
Carbon fiber rod	× 90	168
Ball bearing	× 6	12
TOTAL		300

Table 5.3: Components used on the gimbal system protection and its weight.

5.4.2.3 Dimensioning

The goal of dimensioning is to select the lightest possible springs to absorb the desired energy without failing. There is generally a compromise between the force transferred to the robot's frame, the weight of the external protection and the amount of energy that it can absorb before failure, as well as secondary effects such as available materials, platform dimensions and integration. It is clear that exist a compromise between the outer diameter, inner diameter and the edges of the truncated icosahedron. This relationship is helpful because through it we can determine the value required for each edge to obtain a the final outer shield assembly of the desired diameter. In this case it is required that the external diameter of the polyhedron has a value of 58 cm. Using the equation 5.1 is obtained that each edge should be of 11.7 cm.

$$r_m = \frac{3a}{4}(1 + \sqrt{5}) \tag{5.1}$$

where r_m is the sphere radius ans a is the edge length.

Also, another method to obtain these values was to make a completely design of the helicopter and the protection in Solidworks® (depicted in Figure 5.9a) in order to avoid measurement or assembly errors.

Finally, once followed the above step, the protective frame is directly in contact with obstacles during a collision, and is subject to friction forces that may provoke its rotation. Because the protective frame rotates independently from the inner

frame, the friction force does not affect directly the orientation of the inner frame. The final version design of the proposed solution is depicted in Figure 5.9.

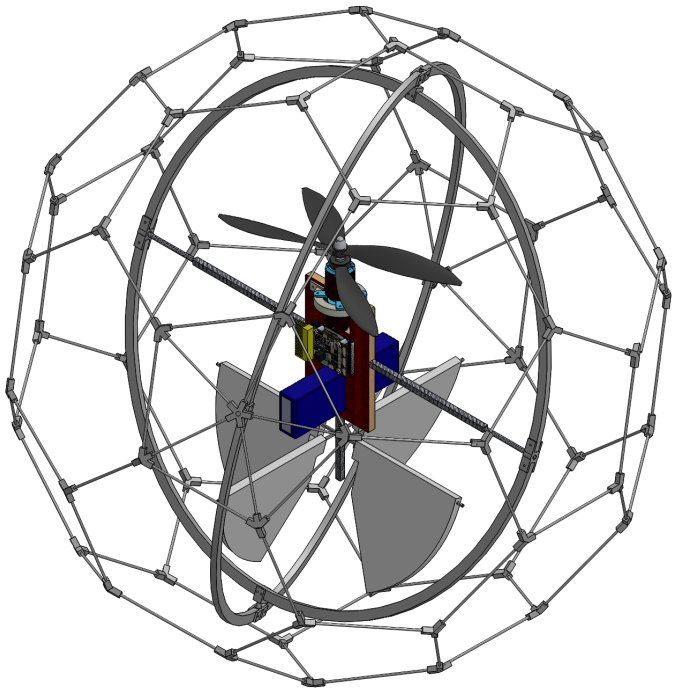

(a) A complete 3D CAD model of the prototype made to avoid measure errors.

(b) The so-called *LaBola* flight robot final assembled version.

Figure 5.9: Comparison: The complete Solidworks® assembly (5.9b) and the plastic and carbon fiber outer frame protection + inner frame drone (5.9b).

6

Concluding Remarks

In this Chapter is summarized the work developed in France at the University of Technology of Compiègne and in Mexico at the Centro de Investigacion y de Estudios Avanzados del Instituto Politécnico Nacional. Due to the variety of topics which involves this work, a section is dedicated to mention the potential applications of such vehicle and the future work to develop.

Contents

6.1 Main Accomplishments and Discussions

The objective of this thesis is to investigate and design a novel configuration flight robot that is capable of flight on wide-open spaces and into the confined, cluttered environments. This thesis has contributed to bring this vision closer to reality by enabling the proposed flight robot to survive to physical exploit contact with their environment. A method for designing protective structures particularly adapted to small flying systems presents a novel way on absorbing collision energy.

A gimbal system protective cage is proposed and implemented on a coaxial platform, which was also designed and built, successfully absorbing energy from head-on collisions. This Archimedean configuration is proposed as a way of protecting the platform in hovering by minimizing the force transmitted to the robot frame while optimizing its weight. When implemented on a hovering platform the mechanism is able to absorb the energy of collisions that would damage or destroy most other flying robots thanks to its rotational property. The design of such a complex machine as the helicopter, requires a broad vision to consider potential problems that will arise, for example: the MAV's configuration and dimensioning, the payload, the size and runtime, these aspects are strongly related to a component: the LiPo battery. The first design the battery was wrongly considered, it was placed on one side of the vehicle which generated a great disturbance because 40% of the total weight of the MAV is due to the battery. Several solutions such as reducing the size of the battery or were analyzed without complying with the three constraints

mentioned above and a second experimental platform were built. Both structures, the gymbal protection and the coaxial helicopter were totally designed and built at the Université de Technologie de Compiégne, partially supported by CONACyT and those are the first contribution of this thesis.

Also, a wide search of the elements (avionics) on-board responsible for the sensing and control of the vehicle was made. For its simplicity and its modularity, the PX4 autopilot was chosen as the brain of the MAV. This leading to a deep study of software because although the PX4 project is considered as an autopilot almost ready to fly, there was no special configuration that was appropriate for the characteristics of the proposed prototype, therefore it was necessary to program a configuration for a coaxial copter.

The second major contribution of this thesis is the non-linear model for a counter-rotating coaxial drone as the non-linear control proposed in Chapter 2 and Chapter 3, respectively. The modeling of the platform is centred on the aerodynamic forces acting in the drone but specially in the thrust force provided by the rotors, such research was motivated by various which use coaxial configuration [32, 36, 39, 52]. The thrust force model is different, then based on work done by the aviation community, a interference factor between the upper rotor and lower rotor is proposed. This result shows that a coaxial vehicle is not as efficient as expected just for the fact of having twin engines, with the same consumption of power provide the same thrust force.

The attitude dynamic of the vehicle is essential since it could present singularities because it will be inside of the protection leaving the Euler-angles unable to

propose a control strategy. Also, it could be possible to work with quaternion representations but due to the ambiguities that it present, a control law in the non-linear manifolds was selected. A research of control strategies was done [93] [71], and a geometric control is proposed to control the drone attitude dynamics. The given control law is a bounded attitude tracking control for *LaBola* which is in the Special Orthogonal Group $\mathsf{SO}(3)$, considering the fact that the actuators have saturation limits. Also, it is shown that the proposed control strategy guarantees exponential stability, and has the capability to track rotational maneuvers with large attitude angles.

Finally, the platform named *LaBola* is presented demonstrating how both collision absorption mechanisms and avionics and aerodynamic actuators can be integrated into a single robot without greatly affecting its aerodynamics and ability to fly. The final and most important contribution of this work is the successful stabilization of such platform and the ability to take off again thanks to small damage suffered after a crash.

6.2 Potential Applications

The results on the design of protective structures as the collision energy absorption shown in this thesis can be applied to almost to any small and compact robotic platform that risks coming into unforeseen, or even planned, contact with objects in its environment, it will depend on many factors as the drone payload and

mission to accomplish. It is adapted to platforms where weight is a critical factor, such as flying robots but can also be applied to ground platforms optimized for maximum endurance. The most likely benefit are other flying platforms such as the quadrotors most commonly used for indoor exploration. Even the most advanced platforms using laser-based SLAM to navigate can benefit the protective structure when their laser scanners fail to detect a window or other indiscernible object.

The most obvious application of the resilient flying robots is the exploration of confined spaces that are dangerous or inaccessible to humans. Typical examples include search and rescue in damaged buildings [87] and mines [7], inspection of nuclear plants and industrial buildings or even the exploration of planets. A flying robot that can take off and land repeatedly in unstructured environments can also be useful as a mobile sensor platform. A payload of 300 g is already sufficient for equipping a variety of sensors such as visible and infrared cameras, thermopiles, gas and temperature sensors or microphones [88] and also is sufficient to install a gimbal system protective cage.

6.3 Future Directions

6.3.1 Advanced Geometric Structure

While this work is presented with a protection using the properties of the gimbal system in the shape of a truncated icosahedron, this geometric shape has, due to its type, very large surfaces without preoteccion and also a large amount of edges and vertices. The first situation can be solved by proposing a geometric shape as much as close to a sphere. To do that, it is useful keeping in mind that a polyhedron close to a sphere shape will increase the number of edges and vertices, therefore, also increase the weight and cost to produce. To avoid this, different protections using various geometric shapes could be done in order to analyse the compromise between the weight and spaces without protection vs the number of edges and vertices. The proposed geometric shapes are the rhombicuboctahedron, the pentakis dodecahedron, the rhombic triacontahedron and the snub cube that are depicted in Figure 6.1. Also a comparative table between them is shown in Table 6.3.1. Furthermore, it will be then necessary to test the vehicle stiffness again to verify the protective plastic and carbon fiber resistance to crashes.

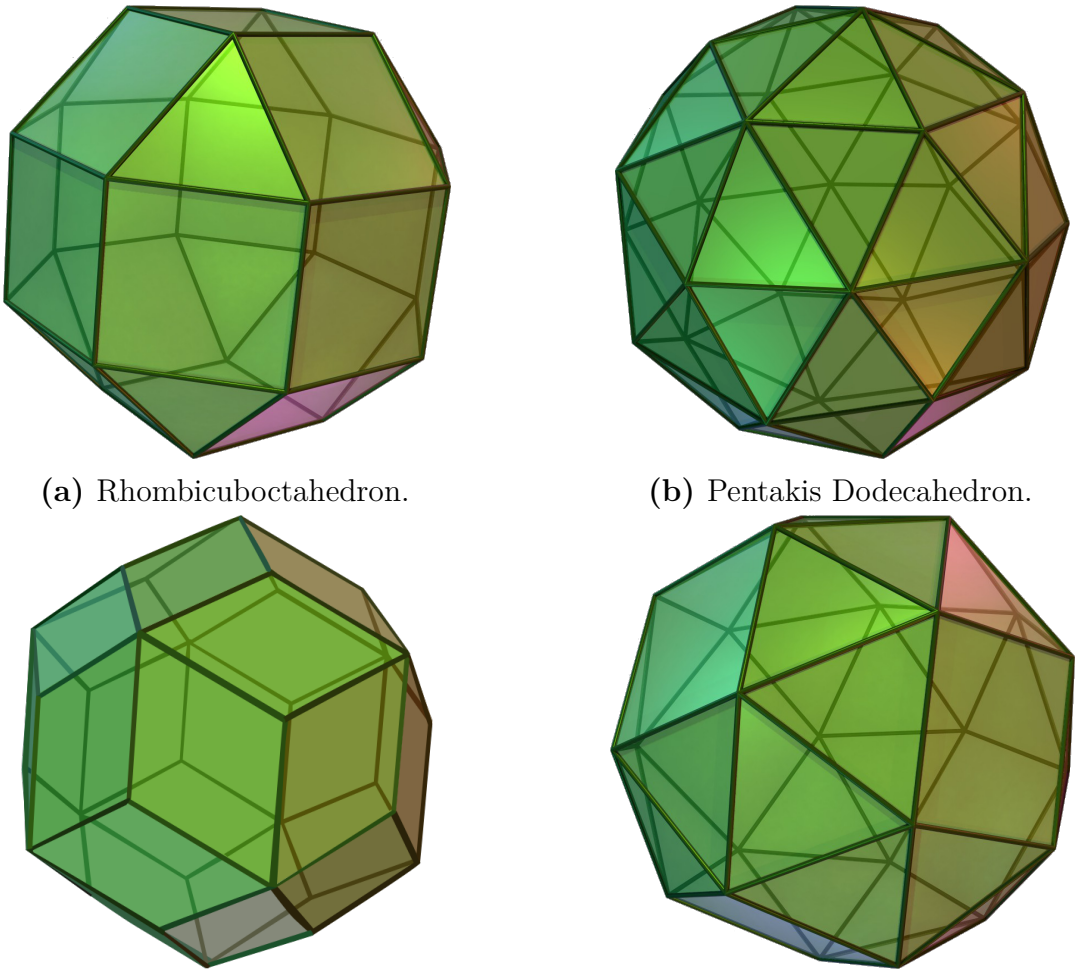

(a) Rhombicuboctahedron.

(b) Pentakis Dodecahedron.

(c) Rhombic Triacontahedron.

(d) Snub Cunbe.

Figure 6.1: 3D geometric shapes that could be done to protect the proposed platform.

Geometric Shape	Edges	Vertices
Rhombicuboctahedron	48	24
Pentakis Dodecahedron	90	32
Rhombic Triacontahedron	60	32
Snub Cube	60	24

Table 6.1: Comparison: Number of edges and vertices present on the possible geometric shapes.

6.3.2 Robotics Implementations and Interaction in Real Environments

Recent works suggests that the next generation of drones will have more interaction with the environment in which they operate entirely by computer vision or using mapping techniques such as SLAM. Knowing this, it is good to think about adapting a camera to the experimental platform developed within this thesis, to implement impact evasion techniques by planning trajectories in real time. For sure, this work involve many others areas did not touched here but this technique together with the gimbal protection would be a strong combination to have a robust obstacles drone.

In the practical sense for the proposed drone, there is a large work to do. At the moment it has been studied and experimented the PX4 autopilot working with the recommended sensors (described in Seccion 5.3.3), thus controlling the position and altitude of a quadrotor besides that the vehicle accomplish missions in autonomous manner using way-points to navigate. With the purpose of investigating and deepen the firmware and applications that brings the autopilot PX4 recorded by default, several experiments were performed in a conventional platform called *ElGuapo*

[87]. The aim of these experiments was to know the behavior of the autopilot in outdoors flights as well as insight into the algorithm that controls the drone in position and altitude.

Such experiments was to give the quadrotor a mission which should make autonomously, i.e., without the intervention of a pilot. To accomplish this mission successfully, it was necessary to use the GPS sensor and telemetry modules described in the subsection 5.3.3 to make it possible to display the variables on board the vehicle. The position control and the mission programming is possible thanks to GPS and ground station QGroudControl [94] in which the way-points followed by the drone are programmed.

The experiment was carried out consists of the following: First, the points are scheduled to follow in the ground station via an interface that displays the map where the drone is; in this case a triangular path formed by 3 main waypoints and with an approximate area of 7.5 m^2 was scheduled. Subsequently, these points are transmitted to the vehicle via Mavlink [95] and recorded in the memory of drone (note that the drone and radio control must be pre-configured to make possible the switch to autonomous mission mode). Once the drone this is in the air, it could be switched to autonomous mission mode so the aerial robot do task. Finally, when the mission ends, the pilot is able to return to manual mode to land the vehicle. This experiment in particular can be seen in `http://youtu.be/WCDix6JT6tY`

Then, the next step then it is transferring this experience to the proposed drone in this thesis taking advantage the PX4 autopilot modularity. Also, taking account the theoretical part, it could be necessary to propose a control law for the vehicle

position.

Bibliography

[1] K. Nonami, F. Kendoul, S. Suzuki, W. Wang, and D. Nakazawa, *Autonomous Flying Robots: Unmanned Aerial Vehicles and Micro Aerial Vehicles*, 1st ed. Springer Publishing Company, Incorporated, 2010.

[2] T. Mueller, *Fixed and Flapping Wing Aerodynamics for Micro Air Vehicle Applications*. American Institute of Aeronautics & Astronautics, 2001.

[3] O. Küng, C. Strecha, A. Beyeler, J.-C. Zufferey, D. Floreano, P. Fua, and F. Gervaix, "The accuracy of automatic photogrammetric techniques on ultra-light uav imagery," in *UAV-g 2011-Unmanned Aerial Vehicle in Geomatics*, 2011.

[4] L. Merino, F. Caballero, J. Martínez-de Dios, J. Ferruz, and A. Ollero, "A cooperative perception system for multiple uavs: Application to automatic detection of forest fires," *Journal of Field Robotics*, vol. 23, no. 3-4, pp. 165–184, 2006.

[5] B. Mendelow, P. Muir, B. Boshielo, and J. Robertson, ""development of e-juba, a preliminary proof of concept unmanned aerial vehicle designed to facilitate the transportation of microbiological test samples from remote rural clinics to national health laboratory service laboratories," *South African Medical Journal*, 2002.

[6] R. D'Andrea, "Guest editorial can drones deliver?" *IEEE Transactions on Automation Science and Engineering*, vol. 11, no. 3, pp. 647–648, July 2014.

[7] B. Pierre-Jean, C. François, V. David, and P. Nicolas, "The navigation and control technology inside the ar.drone micro uav," in *18th IFAC World Congress*, Milano, Italy, 2011, pp. 1477–1484.

[8] R. Murphy, J. Kravitz, S. Stover, and R. Shoureshi, "Mobile robots in mine rescue and recovery," *Robotics Automation Magazine, IEEE*, vol. 16, no. 2, pp. 91–103, June 2009.

[9] J.-C. Zufferey, A. Beyeler, and D. Floreano, "Autonomous flight at low altitutde with vision-based collition avoidance and gps-based path following," presented at the International Conference on Robotics and Automation, Anchorage, Alaska, USA, May 2010.

[10] S. Shen, N. Michael, and V. Kumar, "Autonomous multi-floor indoor navigation with a computationally constrained mav," presented at the International Conference on Robotics and Automation, Shanghai, China, May 2011.

[11] D. Floreano, J. Zufferey, M. V. Srinivasan, and C. Ellington, *Flying Insects and Robots*. Springer, 2009, ch. 6.

[12] M. Blösch, S. Weiss, D. Scaramuzza, , and R. Siegwart, "Vision based mav navigation in unknown and unstructured environments," *Proc.IEEE Int. Conf. on Robotics and Automation*, 2010.

[13] Quanser. (2014) Qball-x4. [Online]. Available: http://www.quanser.com/products/qball

[14] J. F. Roberts, T. Stirling, J.-C. Zufferey, and D. Floreano, "Quadrotor Using Minimal Sensing For Autonomous Indoor Flight," in *European Micro Air Vehicle Conference and Flight Competition (EMAV2007)*, 2007.

[15] W. A. Lewinger, M. Watson, and R. Quinn, "Obstacle avoidance behavior for a biologically-inspired mobile robot using binaural ultrasonic sensors," in *International Conference on Intelligent Robots and Systems, 2006 IEEE/RSJ*, Oct 2006, pp. 5769–5774.

[16] Ascending teechnology website. [Online]. Available: http://www.asctec.de/uav-applications/research/products

[17] G. Wanga, H. Shenga, T. Lub, D. Wanga, and F. Hua, "Development of an autonomous flight control system for small size unmanned helicopter," in *IEEE International Conference on Robotics and Biomimetics, ROBIO 2007.*, Dec 2007, pp. 1804–1809.

[18] F. Sato, "Overview of spherical air vehicle," *Journal of Society of Automotive Engineers of Japan*, pp. 102–103, Mar 2012.

[19] J.-M. Moschetta, "The aerodynamics of micro air vehicles: technical challenges and scientific issues," *Internation Journal of Engineering Systems Modelling and Simulation*, vol. vol. 6, pp. 134–148, 2014.

[20] A. Briod, P. Kornatowski, J.-C. Zufferey, and D. Floreano, "A collision-resilient flying robot," *Journal of Field Robotics*, vol. 31, no. 4, pp. 496–509, 2013.

[21] M. Itasse, J.-M. Moschetta, Y. Ameho, and R. Carr, "Equilibrium transition study for a hybrid mav," *International Journal of Micro Air Vehicles*, vol. 3, no. 4, pp. 229–246, Dec 2011.

[22] A. Kalantari and M. Spenko, "Modeling and performance assessment of the hytaq, a hybrid terrestrial/aerial quadrotor," *Robotics, IEEE Transactions on*, vol. PP, no. 99, pp. 1–7, 2014.

[23] Parrot roling spider website. [Online]. Available: http://www.parrot.com/fr/produits/rolling-spider/

[24] R. Oung and R. D'Andrea, "The distributed flight array," *Mechatronics*, vol. 21, no. 6, pp. 908 – 917, 2011.

[25] A. Klaptocz, "Design of flying robots for collision absorption and self-recovery," Ph.D. dissertation, Ecolé Polytechnique Fédérale de Laussanne, Lausanne, 2012.

[26] D. Aksaray and D. Mavris, "A trajectory tracking algorithm for a hopping rotochute using surrogate models," in *American Control Conference (ACC), 2013*, June 2013, pp. 2000–2005.

[27] P. Castillo, R. Lozano, and A. Dzul, *Modelling and Control of Mini-Flying Machines*. Compiègne, France: Springer, 2005, ch. 1.

[28] J. A. Vilchis, B. Brogliato, A. Dzul, and R. Lozano, "Nonlinear modelling and control of helicopters," *Automatica*, vol. 39, no. 9, pp. 1583 – 1596, 2003.

[29] J.-M. Pflimlin, P. Binetti, P. Souères, T. Hamel, and D. Trouchet, "Modeling and attitude control analysis of a ducted-fan micro aerial vehicle," *Control Engineering Practice*, vol. 18, pp. 209–218, 2010.

[30] A. Dzul, T. Hamel, and R. Lozano, "Modeling and nonlinear control for a coaxial helicopter," in *IEEE International Conference on Systems, Man and Cybernetics, 2002*, vol. 6, Oct 2002.

[31] C. Bermes, S. Bouabdallah, D. Schafroth, and R. Siegwart, "Design of the autonomous micro helicopter mufly," *Mechatronics*, vol. 21, no. 5, pp. 765 – 775, 2011.

[32] A.Drouot, E.Richard, and M.Boutayeb, "Hierarchical backstepping-based control of a gun launched mav in crosswinds: Theory and experiment," *Control Engineering Practice*, vol. 25, no. 20, pp. 16–25, 2014.

[33] D. Schafroth, C. Bermes, S. Bouabdallah, and R. Siegwart, "Modeling and system identification of the mufly micro helicopter," *Journal of Intelligent and Robotic Systems*, vol. 57, no. 1-4, pp. 27–47, 2010.

[34] ——, "Modeling, system identification and robust control of a coaxial micro helicopter," *Control Engineering Practice*, vol. 18, pp. 700–711, 2010.

[35] A. Kostas, H. Christoph, and S. Roland, "Hybrid predictive control of a coaxial aerial robot for physical interaction through contact," *Control Engineering Practice*, vol. 32, pp. 96 – 112, 2014.

[36] F. Wang, S. K. Phang *et al.*, "Nonlinear modeling of a miniature fixed-pitch coaxial uav," presented at the American Control Conference, Montréal, Canada, Jun. 2012.

[37] S. Sheng, A. A. Mian, Z. Chao, and B. Jiang, "Autonomous takeoff and landing control for a prototype unmanned helicopter," *Control Engineering Practice*, vol. 18, no. 9, pp. 1053 – 1059, 2010.

[38] R. Naldi, L. Gentili, L. Marconi, and A. Sala, "Design and experimental validation of a nonlinear control law for a ducted-fan miniature aerial vehicle," *Control Engineering Practice*, vol. 18, pp. 747–760, 2010.

[39] E.S.Espinoza, I. Lugo *et al.*, "Micro helicopter-airplane system: Trajectory tracking and attitude control," presented at the International Conference on Unmanned Aircraft Systems (ICUAS), Atlanta, Georgia, May 2013.

[40] C. Bermes, S. Leutenegger, S. Bouabdallah, D. Schafroth, and R. Siegwart, "New design of the steering mechanism for a mini coaxial helicopter," in *IEEE/RSJ International Conference on Intelligent Robots and Systems, 2008. IROS 2008.*, Sept 2008, pp. 1236–1241.

[41] S. Sheng, A. A. Mian, Z. Chao, and B. Jiang, "Autonomous takeoff and landing control for a prototype unmanned helicopter," *Control Engineering Practice*, vol. 18, no. 9, pp. 1053 – 1059, 2010.

[42] C. P. Coleman, "A survey of theoretical and experimental coaxial rotor aerodynamic research," NASA, CA, Tech. Rep. 3675, Mar. 1997.

[43] T. Koo and S. Sastry, "Output tracking control design of a helicopter model based on approximate linearization," in *Proceedings of the 37th IEEE Conference on Decision and Control, 1998.*, vol. 4, Dec 1998, pp. 3635–3640.

[44] A. Mokhtari and A. Benallegue, "Dynamic feedback controller of euler angles and wind parameters estimation for a quadrotor unmanned aerial vehicle," in *IEEE International Conference on Robotics and Automation, 2004. Proceedings. ICRA '04. 2004*, vol. 3, April 2004, pp. 2359–2366.

[45] S. P. Bhat and D. S. Bernstein, "A topological obstruction to continuous global stabilization of rotational motion and the unwinding phenomenon," *Systems & Control Letters*, vol. 39, no. 1, pp. 63 – 70, 2000.

[46] T. Hamel, R. Mahony, R. Lozano, and J. Ostrowski, "Dynamic modelling and configuration stabilization for an x4-flyer." *15th IFAC Triennial World Congress*, vol. 1, no. 2, p. 3, 2002.

[47] V. Jurdjevic, *Geometric Control Theory*. Cambridge University Press, 1996.

[48] F. Bullo and A. D. Lewis, *Geometric Control of Mechanical Systems*. Springer Verlag, 2004.

[49] D. Maithripala, J. Berg, and W. Dayawansa, "Almost-global tracking of simple mechanical systems on a general class of lie groups," *IEEE Transactions on Automatic Control,*, vol. 51, no. 2, pp. 216–225, Feb 2006.

[50] D. Cabecinhas, R. Cunha, and C. Silvestre, "Output-feedback control for almost global stabilization of fully-actuated rigid bodies," in *47th IEEE Conference on Decision and Control, 2008. CDC 2008.*, Dec 2008, pp. 3583–3588.

[51] N. Chaturvedi, N. McClamroch, and D. Bernstein, "Asymptotic smooth stabilization of the inverted 3-d pendulum," *IEEE Transactions on Automatic Control*, vol. 54, no. 6, pp. 1204–1215, June 2009.

[52] L.Chen and P. J. M. Kerrow, "Modeling the lama coxial helicopter," in *Proceedings of the Australasian Conference on Robotics and Automation*, Brisbane, 2007.

[53] R. Stengel, *Flight Dynamics*. Addison Wesley, 2004.

[54] B. Stevens and F. Lewis, *Aircraft Control and Simulation*. John Wiley and Sons Inc, 1992.

[55] J. G. Leihsman, *Principles of Helicopter Aerodynamics*. Cambridge Univertisy Press, 2006.

[56] A. Bramwell, G. Done, and B. David, *Bramwell's Helicopter Dynamics*. Butterworth-Heinemann, 2001.

[57] W. Johnson, *Helicopter Theory*. Dover Publications Inc, 1994.

[58] G. Xu and M. Chen, "Rotor unsteady aerodynmics reserch of a small-scale coaxial helicopter in hovering state," presented at the International Conference On Computer Desing and Applications (ICCDA), 2010.

[59] C. Yihua, "Nonlinear inverse simulation for the aneuvering flight of coaxial rotor helicopters," *Chinese Journal of Aeronautics*, vol. 10, no. 4, pp. 239–246, 1997.

[60] O. Rand and V. Khromov, "Aerodymic optimization of a coaxial rotor in hover and axial flight," presented at the 27th International Congress of the Areonautics Sciences (ICAS), 2010.

[61] J. Yana and O. Rand, "Performance analysis of a coaxial rotor sysmtem in hover: Three points of view," presented at the 28th International Congress of the Areonautics Sciences (ICAS), 2012.

[62] J. G. Leishman and S. Ananthan, "Aerodynamic optimization of a coaxial proprotor," presented at the 62th Anuual Forum and Technology Display of the American Helicopter Society International, Phoenix, AZN, May 2006.

[63] R. Schlanbuscha, A. Loria, and P. J. Nicklasson, "On the stability and stabilization of quaternion equilibria of rigid bodies," *Automatica*, vol. 48, no. 12, pp. 3135–3141, 2012.

[64] J. T.-Y. Wen and K. Kreutz-Delgado, "The attitude control problem," *IEEE Transactions on Automatic Control*, vol. 36, no. 10, pp. 1148–1162, 1991.

[65] G. M. Hoffmann, H. Huang, S. L. Waslander, and C. J. Tomlin, "Quadrotor helr flight dynamics and control: Theory and experiment," *Proc. of the AIAA Guidance, Navigation, and Control Conference*, vol. 2, 2007.

[66] M. Valenti, B. Bethke, G. Fiore, J. P. How, and E. Feron, "Indoor multi-vehicle flight testbed for fault detection, isolation, and recovery," *Proceedings of the AIAA Guidance, Navigation, and Control Conference and Exhibit, Keystone, CO*, vol. 63, p. 64, 2006.

[67] P. Castillo, A. Dzul, and R. Lozano, "Real-time stabilization and tracking of a four-rotor mini rotorcraft," *IEEE Transactions on Control Systems Technology*, vol. 12, no. 4, pp. 510–516, July 2004.

[68] L. Sanchez, O. Santos, H. Romero, S. Salazar, and R. Lozano, "Nonlinear and optimal real-time control of a rotary-wing uav," in *American Control Conference (ACC), 2012*, June 2012, pp. 3857–3862.

[69] N. Guenard, T. Hamel, and V. Moreau, "Dynamic modeling and intuitive control strategy for an "x4-flyer"," in *International Conference on Control and Automation, 2005. ICCA '05.*, vol. 1, June 2005, pp. 141–146 Vol. 1.

[70] S. Bouabdallah and R. Siegwart, "Backstepping and sliding-mode techniques applied to an indoor micro quadrotor," in *Proceedings of the 2005 IEEE International Conference on Robotics and Automation, 2005. ICRA 2005.*, April 2005, pp. 2247–2252.

[71] T. Lee, "Exponential stability of an attitude tracking control system on so(3) for large-ange rotational maneuvers," *Systems & Control Letters*, vol. 61, pp. 231–237, 2012.

[72] ——, "Robust adaptive attitude tracking on so(3) with an application to a quadrotor uav," *IEEE Transactions on Control Systems Technology*, vol. 21, no. 5, pp. 1924–1930, 2013.

[73] ——, "Geometric tracking control of the attitude dynamics of a rigid body on so(3)," in *American Control Conference 2011*, O'Farrell Street, San Francisco, CA, USA, Jun 2011, pp. 1200–1205.

[74] A. R. Teel, "Global stabilization and restricted tracking for multiple integrators with bounded controls," *Systems & Control Letters*, vol. 18, no. 3, pp. 165–171, 1992.

[75] H. Sussmann, E. Sontag, and Y. Yang, "A general result on the stabilization of linear systems using bounded controls," *IEEE Transactions on Automatic Control*, vol. 39, no. 12, pp. 2411–2425, 1994.

[76] I. Fantoni, A. Zavala, and R. Lozano, "Global stabilization of a PVTOL aircraft with bounded thrust," in *Conference on Decision and Control*, Las Vegas, Nevada, USA, Dec. 2002, pp. 4462–4467.

[77] Himax. (1998) Himax cr2816-1100 contra rotating brushless outrunner motor. Internet datasheet. [Online]. Available: http://www.maxxprod.com/pdf/CR2816.pdf

[78] A. Mystkowski, "Implementation and investigation of a robust control algorithm for an unmanned micro-aerial vehicle," *Robotics and Autonomous Systems*, vol. 62, no. 8, pp. 1187 – 1196, 2014.

[79] E. Cetinsoy, S. Dikyar, C. Hancer, K. Oner, E. Sirimoglu, M. Unel, and M. Aksit, "Design and construction of a novel quad tilt-wing {UAV}," *Mechatronics*, vol. 22, no. 6, pp. 723 – 745, 2012, special Issue on Intelligent Mechatronics.

[80] S. D. Jenie and A. Budiyono, *Automatic Flight Control Systems: Classical approach and modern control perspective*. Bandung Institute of Technology, 2006.

[81] J. M. Sullivan, "Evolution or revolution? the rise of uavs," *IEEE Technology and Society Magazine*, vol. 25, no. 3, pp. 43–49, 2006.

[82] H. Tu and X. Du, "The design of small uav autopilot hardware system based on dsp," in *International Conference on Intelligent Computation Technology and Automation (ICICTA), 2010*, vol. 3, May 2010, pp. 780–783.

[83] U. of Transportation, *Advanced Avionics Handbook*. Washington, DC: Federal Aviation Administration, 2009, ch. 4.

[84] H. Chao, Y. Cao, and Y. Chen, "Autopilots for small unmanned aerial vehicles: A survey," *International Journal of Control, Automation, and Systems*, vol. 8, no. 1, pp. 36–44, 2010.

[85] ETH. (2014) Automatic control laboratory. [Online]. Available: http://control.ee.ethz.ch/

[86] P. Firmware. (2015). [Online]. Available: https://github.com/PX4/Firmware/

[87] G. Flores, "Conception, modélisation et commande d'un drone convertible à quatre hélices pivotantes," thesis, Université de Technologie de Compiègne, Compiègne, France, Oct. 2014.

[88] G. Wanga, H. Shenga, T. Lub, D. Wanga, and F. Hua, "Development of an autonomous flight control system for small size unmanned helicopter," in *IEEE International Conference on Robotics and Biomimetics, 2007. ROBIO 2007.*, Dec 2007, pp. 1804–1809.

[89] M. Itasse, J.-M. Moschetta, Y. Ameho, and R. Carr, "Equilibrium transition study for a hybrid mav," in *Inernational Micro Air Vehicle Conference and Flight Competition*, 2011.

[90] G. Davies and X. Zhang, "Impact damage prediction in carbon composite structures," *International Journal of Impact Engineering*, vol. 16, no. 1, pp. 149 – 170, 1995.

[91] W. Cantwell, P. Curtis, and J. Morton, "Impact and subsequent fatigue damage growth in carbon fibre laminates," *International Journal of Fatigue*, vol. 6, no. 2, pp. 113 – 118, 1984.

[92] C. Creighton and T. Clyne, "The compressive strength of highly-aligned carbon-fibre/epoxy composites produced by pultrusion," *Composites Science and Technology*, vol. 60, no. 4, pp. 525 – 533, 2000.

[93] F. Goodarzi, D. Lee, and T. Lee, "Geometric nonlinear pd control for a quadrotor uav on so(3)," presented at the European Control Conference, Zurich, Switzerland, Jul. 2013.

[94] Q. Control. (2014). [Online]. Available: http://qgroundcontrol.org/

[95] M. Protocol. (2014). [Online]. Available: http://qgroundcontrol.org/mavlink/start